# Turbulent intensity and Reynolds number effects on an airfoil at low Reynolds numbers

Cite as: Phys. Fluids **26**, 115107 (2014); https://doi.org/10.1063/1.4901969
Submitted: 24 February 2014 . Accepted: 31 October 2014 . Published Online: 24 November 2014

S. Wang, Y. Zhou, Md. Mahbub Alam, and H. Yang

PHYSICS OF FLUIDS **26**, 115107 (2014)

# Turbulent intensity and Reynolds number effects on an airfoil at low Reynolds numbers

S. Wang,[1] Y. Zhou,[2,a)] Md. Mahbub Alam,[2] and H. Yang[3]
[1]*Department of Mechanical Engineering, The Hong Kong Polytechnic University, Hung Hom, Kowloon, Hong Kong*
[2]*Institute for Turbulence-Noise-Vibration Interaction and Control, Shenzhen Graduate School, Harbin Institute of Technology, Shenzhen, China*
[3]*Department of Building Services Engineering, The Hong Kong Polytechnic University, Hung Hom, Kowloon, Hong Kong*

(Received 24 February 2014; accepted 31 October 2014; published online 24 November 2014)

This work investigates the aerodynamics of a NACA 0012 airfoil at the chord-based Reynolds numbers ($Re_c$) from $5.3 \times 10^3$ to $2.0 \times 10^4$. The lift and drag coefficients, $C_L$ and $C_D$, of the airfoil, along with the flow structure, were measured as the turbulent intensity $T_u$ of oncoming flow varies from 0.6% to 6.0%. The analysis of the present data and those in the literature unveils a total of eight distinct flow structures around the suction side of the airfoil. Four $Re_c$ regimes, i.e., the ultra-low ($<1.0 \times 10^4$), low ($1.0 \times 10^4$–$3.0 \times 10^5$), moderate ($3.0 \times 10^5$–$5.0 \times 10^6$), and high $Re_c$ ($>5.0 \times 10^6$), are proposed based on their characteristics of the $C_L$-$Re_c$ relationship and the flow structure. It has been observed that $T_u$ has a more pronounced effect at lower $Re_c$ than at higher $Re_c$ on the shear layer separation, reattachment, transition, and formation of the separation bubble. As a result, $C_L$, $C_D$, $C_L/C_D$ and their dependence on the airfoil angle of attack all vary with $T_u$. So does the critical Reynolds number $Re_{c,\mathrm{cr}}$ that divides the ultra-low and low $Re_c$ regimes. It is further noted that the effect of increasing $T_u$ bears similarity in many aspects to that of increasing $Re_c$, albeit with differences. The concept of the effective Reynolds number $Re_{c,\mathrm{eff}}$ advocated for the moderate and high $Re_c$ regimes is re-evaluated for the low and ultra-low $Re_c$ regimes. The $Re_{c,\mathrm{eff}}$ treats the non-zero $T_u$ effect as an addition of $Re_c$ and is determined based on the presently defined $Re_{c,\mathrm{cr}}$. It has been found that all the maximum lift data from both present measurements and previous reports collapse into a single curve in the low and ultra-low $Re_c$ regimes if scaled with $Re_{c,\mathrm{eff}}$. © *2014 AIP Publishing LLC*. [http://dx.doi.org/10.1063/1.4901969]

## I. INTRODUCTION

Investigations on the aerodynamics of airfoils are traditionally driven by the need of aeronautical applications and are focused on the flow of small angle of attack ($\alpha$), i.e., the pre-stalled condition, and the chord Reynolds number $Re_c \equiv U_\infty c/\nu$ is largely over $5 \times 10^5$, where $U_\infty$ is the free-stream velocity, $c$ is the airfoil chord length, and $\nu$ is the fluid kinematic viscosity. The knowledge obtained is now inadequate due to developments in small wind turbines, small unmanned aerial vehicles (UAVs) such as micro air vehicles (MAVs), nano air vehicles (NAVs), and increasing interests in understanding bird and insect flights.[1–3] All these activities involve very low $Re_c$. For instance, the $Re_c$ is commonly less than $2 \times 10^5$ for MAVs,[4] less than $1.5 \times 10^4$ for NAVs,[5] and even lower for insect flights.[6] In the study of the airfoil wake, $Re_c \lesssim 5 \times 10^5$ is often called the low Reynolds number because of the occurrence of reattachment after laminar separation, which forms the so-called laminar separation bubble (LSB).[7] At $Re_c < 1 \times 10^4$, the separated boundary layer is

a)Author to whom correspondence should be addressed. Electronic mail: zhouyu@hitsz.edu.cn

 

characterized by a delayed transition and remains laminar for a rather long longitudinal distance, not prone to reattachment, implying the absence of the LSB or a qualitative change in the flow structure.[8] It is well known that an airfoil may stall given an adequately large $\alpha$, which is associated with the burst of the separation bubble and a rapid drop in the lift coefficient $C_L$ for a small increase in $\alpha$. However, at $Re_c < 1 \times 10^4$, the typical feature of stall – the rapid drop in $C_L$ does not occur due to the absence of the separation bubble,[9] which is referred to as the ultra-low Reynolds number.[8,10]

Developments in small wind turbines may involve not only small $Re_c$ but also large $\alpha$. At the starting stage of small wind turbines, $Re_c$ increases from $10^4$ to $10^5$ and $\alpha$ may change over the range of 0°–90°. Furthermore, the turbulence level $T_u$ ($\equiv u'_{\rm rms}/\overline{U}$) of wind often varies from time to time, where overbar and subscript rms denote the local mean and root mean square values of the instantaneous streamwise velocity $U$ and its fluctuating component $u'$, respectively. For example, in coastal or typhoon-affected areas, wind turbine blades may be under strongly turbulent high winds. Naturally, there is a strong need to understand the effect of $T_u$ on the low $Re_c$ airfoil at a large $\alpha$.

The effect of $T_u$ on airfoil aerodynamics has received considerable attention in the literature for the low-to-high $Re_c$ range; this effect is largely associated with the stall, increasing the stall angle or the maximum $C_L$.[11–14] Hoffmann[12] measured $C_L$ and drag coefficient $C_D$ of NACA 0015 airfoil at $Re_c = 2.5 \times 10^5$. He found that a variation in $T_u$ from 0.25% to 9.0% resulted in an increase in the maximum of $C_L$ by 30%. Similar conclusions were made experimentally by Mish and Devenpor[13] and numerically by Gilling *et al.*[14] for NACA 0015 airfoils at $Re_c = 1.17 \times 10^6$ and $1.6 \times 10^6$, respectively. Huang and Lee[15] investigated the $T_u$ effect on both aerodynamic loads and surface-flow characteristics of the NACA 0012 airfoil at $Re_c = 0.5 \times 10^5$ to $1.5 \times 10^5$, with $T_u$ varying between 0.20% and 0.65%. It was found that an increase in $T_u$ at $T_u < 0.45\%$ could effectively delay the stall. The effect of $T_u$ on the maximum $C_L$ became significant for $T_u > 0.45\%$. Investigations on other airfoils, such as NACA $65_4$-421 and HQ 17,[16,17] showed a similar dependence on $T_u$.

One may question whether the previously obtained knowledge of the $T_u$ effect on flow at $Re_c > 0.5 \times 10^5$ could be extrapolated to the low- and ultra-low $Re_c$ flow, i.e., $Re_c < 0.5 \times 10^5$. This extrapolation is naturally not recommendable in view of the difference, discussed above, in the flow structure about the airfoil between the regimes of high-, low-, and ultra-low $Re_c$. This work aims to investigate experimentally the $T_u$ effect on the aerodynamics of a NACA 0012 airfoil at low- and ultra-low $Re_c$. Three levels of $T_u$, i.e., 0.6%, 2.6%, and 6.0%, have been examined over $\alpha = 0°$–$25°$ for $Re_c = 5.3 \times 10^3$ and $2.0 \times 10^4$, which represent the ultra-low- and low-$Re_c$ regimes, respectively. Experimental details are given in Sec. II. Results are presented and discussed in detail in Secs. III–V. This work is concluded in Sec. IV.

## II. EXPERIMENTAL DETAILS

### A. Water tunnel, test model, and turbulence generator

Experiments were performed in a closed-loop water tunnel, with a test section of 0.3 m (width) × 0.6 m (height) × 2.4 m (length). The water speed in the test section ranges from 0.05 to 4 $\rm ms^{-1}$. The flow non-uniformity is less than 0.1%. The tunnel was described in detail by Wang *et al.*[18] A NACA 0012 airfoil, with a span length of $s = 0.27$ m and $c = 0.1$ m, was used as the test model and mounted horizontally in the test section. The angle of attack was adjustable by rotating the airfoil supporting shaft, 0.4 $c$ away from the leading edge (Fig. 1(a)), with a maximum uncertainty of 0.5°. One endplate was mounted on each side of the model to minimize the end effect (Fig. 1(c)). Measurements were conducted at free-stream velocity $U_\infty = 0.053$ and 0.200 $\rm ms^{-1}$, corresponding to $Re_c = 5.3 \times 10^3$ and $2.0 \times 10^4$, respectively. At these speeds, $T_u$ was measured to be about 0.6%.

The higher $T_u$ was achieved by placing a grid upstream of the airfoil model. The characteristic dimensions of the grid are $M = 40$ mm, $D = 10$ mm, and $H = 40$ mm, with a porosity of 64% (Fig. 1(b)). The grid was installed at the end of the tunnel contraction section, generating the closely uniform and isotropic turbulence.[15,19] Laser Doppler anemometer (LDA) was used to measure the flow velocity with flow seeded with the polyamide particles of 20 $\mu$m in diameter. The LDA measurement accuracy depends on seeding particles, and is adversely influenced by impurities that are inevitably present in natural water. At present low flow speeds, this accuracy is adequate for

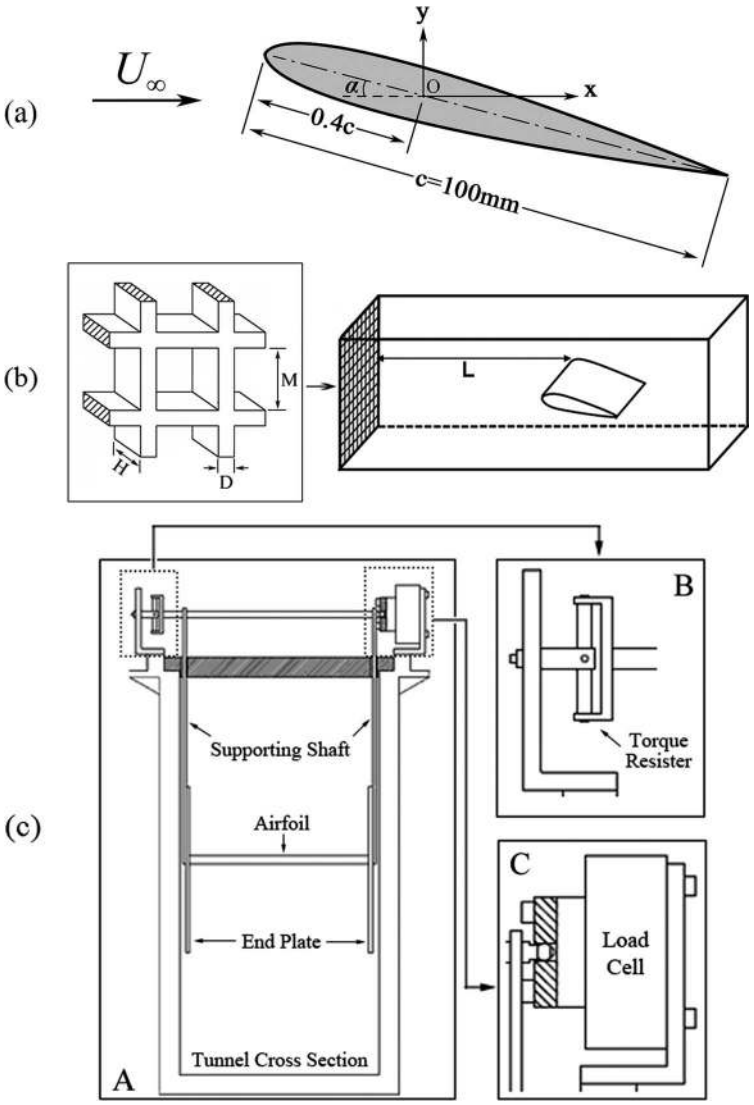


FIG. 1. (a) Airfoil model and definition of the coordinate system; (b) schematic of grid and airfoil installation in the water tunnel; (c) setup of force measurement: (A) Cross-sectional view. (B) Torque resister. (C) Load cell.

measuring the mean velocity, but not for the fluctuating velocity. As such, a LDA-calibrated hot-film probe, sensitive to velocity fluctuation, was used to measure $T_u$. The measurement uncertainties of both mean and fluctuating velocities are estimated to be within 1% based on 10 repeated tests.

A variation in $T_u$ was achieved by changing distance $L$ from the grid to the airfoil model (Fig. 1(b)). The choice of $L$ is based on two considerations, i.e., the uniformity of $\overline{U}$ and suitable $T_u$. $U$ was measured using LDA at a number of points along the z direction in the y-z plane to estimate the uniformity of $\overline{U}$ and $T_u$. As shown in Fig. 2(a), there is a discernible variation in $\overline{U}$ across the flow at $L = 10$ M but not so at $L = 14$ M. A parameter $I_u$ ($\equiv u''_{\rm rms}/\langle\overline{U}\rangle$) is defined to quantify the departure from the perfect uniformity, where $\langle\overline{U}\rangle$ represents the averaged $\overline{U}$ across the flow and $u''$ is the variation of $\bar{U}$ about the average. Both $T_u$ and $I_u$ decay with increasing $L$, following a power law (Fig. 2(b)). Three free-stream turbulence levels, i.e., $T_u = 6.0\%$, 2.6%, and 0.6%, of the flow (I) were obtained at $L = 14$ M and 41 M and removing the turbulence generator, respectively, all with $I_u$ less than 1%. According to Table I, $u'_{\rm rms}/v'_{\rm rms}$ was less than 1.2, showing a quasi-isotropic freestream turbulence for all the three $T_u$ levels, where $v'$ is the fluctuating component of the lateral instantaneous velocity. Based on the Taylor hypothesis, the streamwise integral length scales $L_u^x$

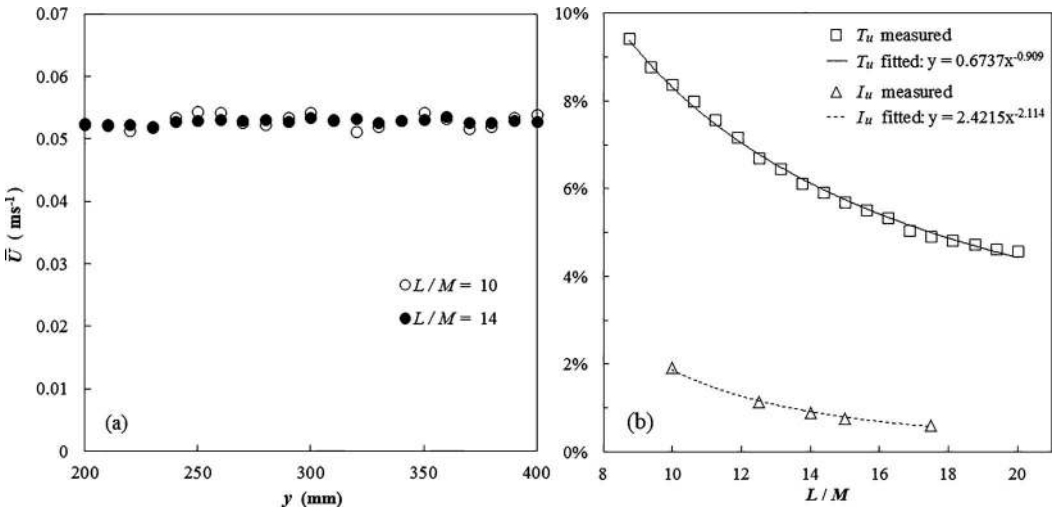


FIG. 2. (a) The distribution of $\bar{U}$ at $L/M = 10$ and 14; (b) dependence of streamwise turbulence intensity $T_u$ and inhomogeneity $I_u$ ($\equiv u''_{\rm rms}/\langle\bar{U}\rangle$) on $L/M$.

could be estimated by $L_u^x = \bar{U}\int_0^{\tau_0} R_u(\tau)d\tau$, where $R_u$ is the autocorrelation functions of single point temporal fluctuating streamwise velocity, $\tau$ is the time difference, and $\tau_0$ is where $R_u$ equals the first zero. $L_u^x$ was $0.16c$ and $0.25c$ at $T_u = 6.0\%$ and 2.6%, respectively. The $L_u^x$ of the order of magnitude of $c$ means that the inflow conditions are steady and the flow is turbulent on the airfoil.[20] Figure 3 presents the power spectrum of streamwise velocity in the freestream. The magnitude of the power spectrum increases with $T_u$ for all frequencies and no prominent peak can be seen, irrespective of the $T_u$ level, ensuring the airfoil not affected by fluctuations at a particular frequency.

## B. Force measurements

Figure 1(c) shows the setup of the force measurement system, which was modified from that of Alam *et al.*[8] to accommodate a new load cell model of higher resolution. The fluid force on the airfoil and its endplates was transmitted to the load cell installed above water via the supporting shaft, as shown in part A. The force resulted in a torque, influencing the output of the load cell. To minimize this influence, a torque-resistor, marked by part B, was deployed, which was fixed at one connection pole. The end of the connection pole on the load cell side could freely rotate relatively to the cell, marked by part C, thus allowing the force to be transmitted to the cell but not the torque. One calibrated Kyowa WGA-800c load cell with a measuring range of ±10N was used to measure

TABLE I. Characteristics of the free-stream flow.

| No. | Grid | $L/M$ [a] | $I_u$ (%) [b] | $T_u$ (%) [c] | $u'_{\rm rms}/v'_{\rm rms}$ [d] | $L_u^x/c$ [e] |
|---|---|---|---|---|---|---|
| 1 | No | ... | 0.26 | 0.6 | 1.06 | ... |
| 2 | Yes | 41 | 0.35 | 2.6 | 1.22 | 0.25 |
| 3 | Yes | 14 | 0.90 | 6.0 | 1.18 | 0.16 |

[a] $L$ is the downstream distance of airfoil model from the gird and $M$ is the grid mesh size.
[b] $I_u$ is the uniformity of the free-stream flow.
[c] $T_u$ is the turbulence intensity of the free-stream flow.
[d] $u'_{\rm rms}$ and $v'_{\rm rms}$ are the rms of the fluctuation components of intantanous streamwise and lateral velocities, respectively.
[e] $L_u^x$ is the streamwise integral length scale of the free-stream flow.

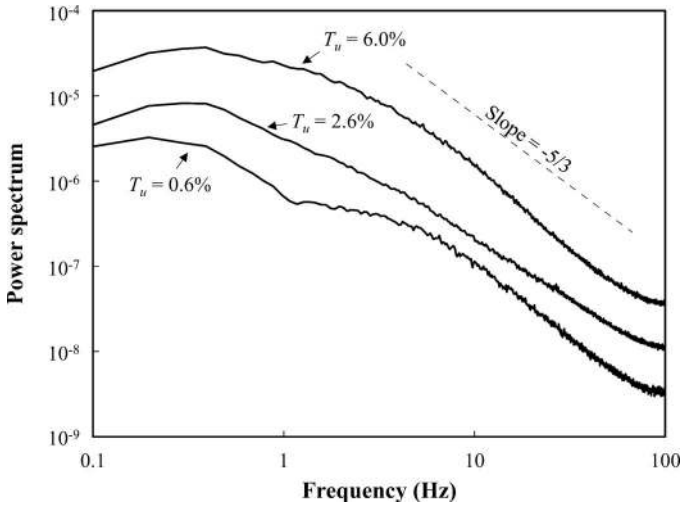


FIG. 3. Power spectrum of freestream streamwise velocity for different $T_u$.

the lift and drag forces, $F_L$ and $F_D$. The lift and drag coefficients are calculated by

$$C_L = \frac{F_L}{\frac{1}{2}\rho U_\infty^2 cs}, \tag{1}$$

$$C_D = \frac{F_D}{\frac{1}{2}\rho U_\infty^2 cs}, \tag{2}$$

where $\rho$ is the fluid density. The measured force signals were amplified and low-pass-filtered at the cutoff frequency of 10 Hz before being sampled at 30 Hz through an A/D board. The sampling duration was 5 min. The resolution of the load cell is within 0.002 N, resulting in the uncertainties of less than 5% in the estimate of $C_D$ and $C_L$. For $\alpha = 0^\circ$–$25^\circ$, the blockage ratio of the airfoil ranges from 2% to 7.8%. Correction is made for both $C_L$ and $C_D$ for all angles, following Maskell[21] and Barlow *et al.*[22] Since the correction tends to fail for a blockage of higher than 6%,[22] additional errors may occur in both $C_L$ and $C_D$ at $\alpha > 20^\circ$. As a result, present $C_L$ and $C_D$ at $\alpha = 25^\circ$ tend to be larger than the actual value in the absence of blockage. No further correction is attempted due to a lack of reliable methods. Indeed, $\alpha > 20^\circ$ is well beyond the stall, which is not the focus of the present investigation.

### C. LIF flow visualization

A laser induced fluorescent (LIF) flow visualization system was used to visualize the airfoil wake at $Re_c = 5.3 \times 10^3$ in the $x$-$y$ plane through the airfoil mid-span, that is thought to be representative of the whole span, as the endplates installed made the flow two dimensional.[8,23] A pin hole of 1.0 mm in diameter was drilled at the airfoil leading edge for the release of dye (Rhodamine 6G 99%). The flow marker or dye was stored in a small tank placed at about 1 m above the airfoil. The tank was connected to the airfoil via a rubber tube. A regulator valve was used to control the flow rate of dye. A laser beam from a 6W argon ion laser source (Spectra Physics) was transmitted through an optic fibre and transformed into a plane sheet using a laser-sheet probe. The visualized flow images were recorded using a Sony video camera (DCR-PC100E) with a framing rate of 25 frames/s.

### D. Particle image velocimetry (PIV) measurements

A Dantec PIV system (PIV2100) was used to measure flow in the $x$-$y$ plane at mid-span of the airfoil (Fig. 1(a)). The airfoil was made of transparent plexiglas, allowing the flow field of interest to be visualized without shadow except a passage for dye injection. The same flow seeding as in the

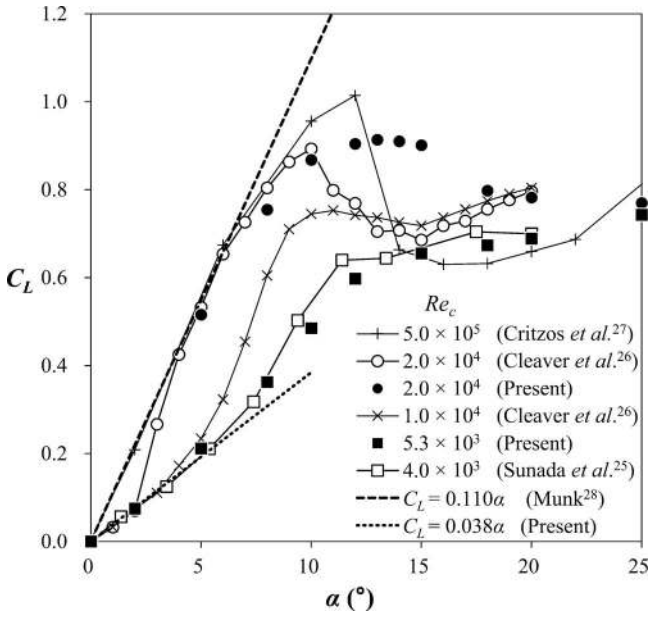


FIG. 4. Comparison in $C_L$ between present and previous measurements for NACA 0012.

LDA measurements was used. The PIV image size was 2048 × 2048 pixels, covering an area of 226 mm × 226 mm. In image processing, an interrogation window of 8 × 8 pixels was used with 50% overlap in each direction. The ensuing in-plane velocity fields consisted of 511 × 511 vectors. The number of erroneous vectors in the captured flow field was about 443, corresponding to 0.17% of the total. These erroneous vectors occur due to insufficient light intensity in the shadow of the dye injection passage built in the airfoil model. The moving-average validation built into the data processing software of Dantec PIV was used to reject erroneous vectors. The rejected vectors were replaced by vectors interpolated from surrounding vectors. See Host-Madsen and McCluskey[24] for more details. About 450 images with good convergence were captured for each test case to estimate the iso-contours of $\overline{U}$.

## III. REYNOLDS NUMBER EFFECT

The measured $C_L$ at $T_u = 0.6\%$ is compared with the published data for $Re_c = 4.0 \times 10^3$–$5.0 \times 10^5$ in Fig. 4. All the data have a $T_u$ value of $\leq 1\%$ and flow is nominally two-dimensional. The present results are in general in good agreement with those of comparable $Re_c$. All the $C_L$ data at $Re_c = 1.0 \times 10^4$ or more exhibit a rise-and-fall behaviour, i.e., the occurrence of stall. The present $C_L$ at $Re_c = 5.3 \times 10^3$ however does not show the rise-and-fall behaviour, which is refered here and after as the absence of stall, as noted by Sunada *et al.*[25] at $Re_c = 4.0 \times 10^3$. A similar observation was also reported by Alam *et al.*[8] The present $C_L$ at $Re_c = 2.0 \times 10^4$ agrees well before the stall angle with Cleaver *et al.*[26] at the same $Re_c$. However, there is a discrepancy in $\alpha$ for the occurrence of the stall, at least partially due to a lower $T_u$ (<0.5%) in measurement of Cleaver *et al.*[26] A lower $T_u$ corresponds to a smaller stall angle.[11–14] Furthermore, their measurement had a blockage ratio of more than 6% for $\alpha > 13°$, but no information was given on whether the data were corrected, which should also contribute to the discrepancy. Two more sets of the $C_L$ data, i.e., $Re_c = 1.0 \times 10^4$ from Cleaver *et al.*[26] and $5.0 \times 10^5$ from Critzos *et al.*,[27] are included in Fig. 4 to facilitate the discussion on the influence of $Re_c$ on the $C_L$ variation with $\alpha$.

### A. Dependence of $C_L$ on $\alpha$ and underlying flow physics

The $C_L$ dependence on $\alpha$ exhibits a marked change in slope with $Re_c$ varying. For $Re_c = 5.0 \times 10^5$, $C_L$ increases linearly from $\alpha = 0°$ to 6° with an initial slope of 0.110 (or $2\pi$ if radian is used as

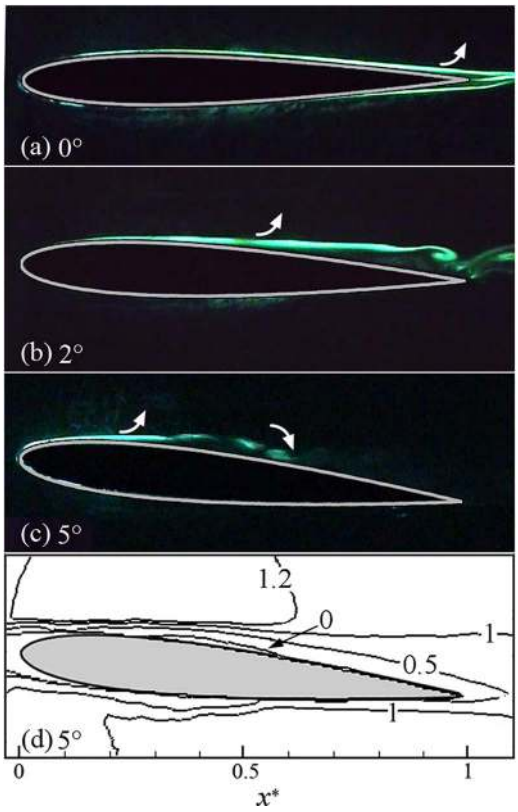


FIG. 5. Typical photographs captured in LIF flow visualization: (a) $\alpha = 0°$, (b) 2°, (c) 5°, (d) the iso-contours of PIV-measured $\overline{U}^*(\alpha = 5°)$. $Re_c = 2.0 \times 10^4$. Symbols ↗ and ↘ indicates the occurrence of flow separation and reattachment, respectively.

unit of $\alpha$), as predicted theoretically based on inviscid thin airfoil theory.[28] As $Re_c$ is reduced to $2.0 \times 10^4$, $C_L$ shows a different initial slope of about 0.038 from $\alpha = 0°$ to 2° but then recovers rapidly in a nonlinear manner. This nonlinear variation at small $\alpha$ was observed by Panda and Zaman[29] and by Laitone[30] for NACA 0012 at $Re_c = 2.0 \sim 4.0 \times 10^4$ and by Lutz *et al.*[31] for NACA 0009 at $Re_c = 5.0 \times 10^4$. As flow visualization photographs (Figs. 5(a) and 5(b)) indicate, the boundary layer over the airfoil with $\alpha = 0°$–2° is laminar at $Re_c = 2.0 \times 10^4$, and flow separation occurs near the trailing edge on the suction side of airfoil, without reattachment. On the other hand, the separated flow reattaches at $\alpha > 2°$, producing a separation LSB, as illustrated in Fig. 5(c). More details of the separation bubble, enclosed by the contour of $\overline{U}^* = 0$ and the airfoil surface, for the same $\alpha$ are evident from the iso-contours of the PIV-measured $\overline{U}^*$ (Fig. 5(d)). Asterisk denotes normalization by $c$ and/or $U_\infty$ in this paper. Note that the transition in the shear layer occurs prior to reattachment (Fig. 5(c)). Correspondingly, $dC_L/d\alpha$ reduces from $\alpha = 3°$ to 9°, where the transition takes place between flow separation and reattachment. In the absence of reattachment ($\alpha > 9°$), $dC_L/d\alpha$ drops to a negative value and then increases. These observations imply that a simplified correlation of $dC_L/d\alpha$ and its underlying flow state could be found when taking the nonlinear $C_L$ dependence on $\alpha$ as piecewise linear segments.

A lower $Re_c$ ($=1.0 \times 10^4$) enables the initial linear range to be extended to $\alpha = 3°$, and then incurs a recovery in $C_L$ up to $\alpha = 10°$, which is associated with an increasing slope from $\alpha = 3°$ to 7° but then decreasing up to $\alpha = 10°$, that is, $\alpha = 7°$ is the inflection point. The separation bubble is formed in both ranges of $\alpha$, though exhibiting distinct features. At $\alpha = 3°$–7°, the shear layer transition occurs after reattachment; as such, the bubble is long and laminar, all the way from separation to reattachment. On the other hand, at $\alpha = 7°$–10°, the transition takes place between flow separation and reattachment; the bubble is shorter and partially laminar, that is, laminar separation

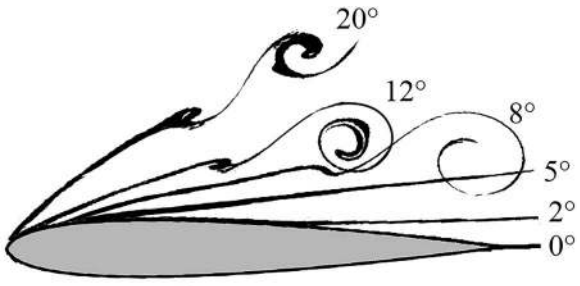


FIG. 6. Instantaneous separated shear layers at different $\alpha$ (extracted from LIF flow visualization photographs). $Re_c = 5.3 \times 10^3$.

followed by turbulent reattachment. Apparently, the inflection point $\alpha = 7^\circ$ is a turning point, where the transition occurs at reattachment. As noted in the previous paragraph, at $Re_c = 2.0 \times 10^4$, the bubble where the transition occurs before reattachment corresponds to reducing $dC_L/d\alpha$ from $\alpha = 3^\circ$ to $9^\circ$. It may be inferred that the starting $\alpha$ for this bubble type is larger at smaller $Re_c$ ($\alpha = 3^\circ$ at $Re_c = 2.0 \times 10^4$; $\alpha = 7^\circ$ at $Re_c = 1.0 \times 10^4$), in agreement with our intuition.

As $Re_c$ decreases to $5.3 \times 10^3$ and $4.0 \times 10^3$, the initial linear range of $C_L$ versus $\alpha$ is extended further to $\alpha = 5^\circ$, and then $C_L$ varies almost linearly up to $\alpha = 12^\circ$ with a larger slope. In both $\alpha$ ranges, the separated flow does not reattach. The different slopes are linked to the fact that the shear layer is elongated, rolling up behind the trailing edge, in the former but rolls up over the airfoil surface in the latter (Fig. 6), with rolling up position moving upstream with $\alpha$. The drastic drop in $C_L$ does not crop up in the remaining $\alpha$ examined, implying the absence of stall and the absence of reattachment of the separated flow over the entire $\alpha$ range examined. The above observations are confirmed by flow visualization data. Typical photographs (Fig. 6) show that the separation point shifts gradually towards the leading edge without flow reattachment from $\alpha = 0^\circ$ to $20^\circ$. In this $\alpha$ range, the recovery of $C_L$ towards the theoretical $0.110\alpha$ is due to (i) boundary layer separation shifted towards the leading edge, (ii) upstream shift of shear-layer rollup, and (iii) transition of the shear-layer/wake from laminar to turbulent shifted towards the separation point. While point (i) makes a predominant contribution to increasing lift for $\alpha \leq 5^\circ$, points (ii) and (iii) produce additional contribution for lift increase over $5^\circ < \alpha \leq 12^\circ$. However, all these mechanisms are feeble for $\alpha > 12^\circ$. The curve therefore displays a turning point at $\alpha \approx 12^\circ$ after which the increase in $C_L$ is slowed down with increasing $\alpha$. The observation is rather similar to that found for inclined plates at $Re_c = 4.0 \times 10^3$ by Sunada *et al.*[25]

In summary, the $C_L$ dependence on $\alpha$ up to the pre-stall is characterized at $Re_c = 2.0 \times 10^4$ by two distinct behaviours, (i) a constant $dC_L/d\alpha$ (=0.038) at small $\alpha$, associated with laminar flow separation without reattachment, and (ii) a decreasing $dC_L/d\alpha$ at larger $\alpha$ linked to laminar flow separation followed by turbulent reattachment. At $Re_c = 1.0 \times 10^4$, other than behaviours (i) and (ii), the $C_L$ dependence displays one more distinct behaviour, that is, (iii) an increasing $dC_L/d\alpha$ due to laminar separation followed by laminar reattachment at $\alpha = 3^\circ$–$7^\circ$. With decreasing $Re_c$, the $\alpha$ range over which behaviour (i) occurs is enlarged and that corresponding to (ii) shrinks. By $Re_c \approx 5.3 \times 10^3$ or lower, the $C_L$ dependence consists of two linear variations connected to shear layer rollup behind the trailing edge and over the surface, respectively.

### B. Classification of the $Re_c$ regimes

A significant $Re_c$ effect on $C_L$ is also reflected in a variation in the maximum $C_L$, i.e., $C_{L,\max}$. The $C_{L,\max}$ is an important parameter in terms of the performance of an airfoil. It has been well established that $C_{L,\max}$ strongly depends on $Re_c$ for large $Re_c$.[23,32–34] Fig. 7 presents a collection of $C_{L,\max}$ of NACA 0012 for a wide range of $Re_c$ in the literature [25,26,35–39] as well as the present measurement. In the absence of stall, $C_L$ will reach its global maximum at $\alpha \approx 40^\circ$.[8] However, in order to compare the lift performance within stall $\alpha$ range, $C_{L,\max}$ is defined in such case as the

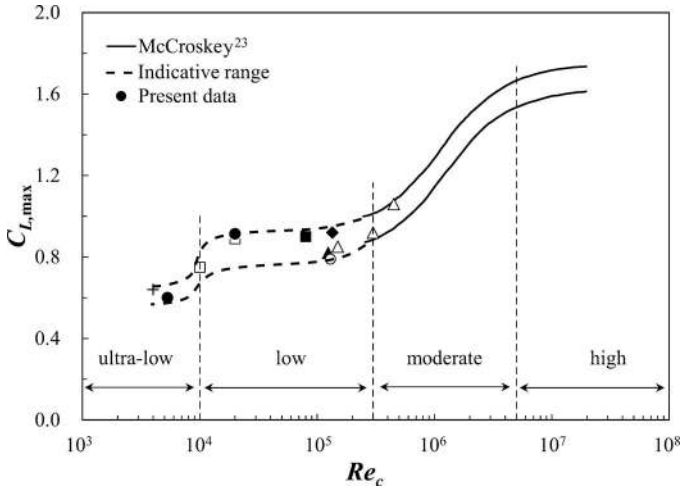


FIG. 7. Dependence of $C_{L,\max}$ on $Re_c$ of NACA 0012 airfoil: + Sunada *et al.*[25]; ■ Chen and Choa[35]; □ Cleaver *et al.*[26]; ◯ Grager *et al.*[36]; ♦ Lee and Gerontakos[37]; ▲ Wong and Kontis[38]; △ Sant and Ayuso.[39]

point at which $C_L/\alpha$ reaches maximum. $C_L$ increases very slowly with $\alpha$ after this turning point. The dependence of $C_{L,\max}$ on $Re_c$ from McCroskey[23] is given to cover the moderate and high $Re_c$ range. A relatively large scattering is expected over the low $Re_c$ range because of different experimental conditions. In general, $C_{L,\max}$ grows with increasing $Re_c$. However, the increasing rate can be very different for different $Re_c$ ranges. As such, four Reynolds number regimes may be identified in terms of the dependence of $C_{L,\max}$ on $Re_c$, each associated with distinct flow physics behind.

The ultra-low Reynolds number regime refers to $Re_c < 1 \times 10^4$. The term the ultra-low Reynolds number was first used by Kunz and Kroo[10] and then by Alam *et al.*[8] and Zhou *et al.*[9] In this $Re_c$ range, $C_{L,\max}$ is small, about 0.6; the boundary layer is laminar and separates at small $\alpha$, e.g., $\alpha < 2^\circ$ for $Re_c = 5.3 \times 10^3$. The separated shear layer remains laminar for a prolonged distance without reattachment and hence without any separation bubble formed. As a result, stall is absent. With an increase in $\alpha$, an enhancement in $C_L$ results mainly from a shift in the shear layer separation and rollup towards the leading edge and a shift in transition from laminar shear layer to turbulent on the suction side towards the separation point. All the shifts make positive contribution to $C_L$, though the separation point change contributes predominantly at $\alpha \leq 5^\circ$ and the other two at $\alpha > 5^\circ$. Thus, the $C_{L,\max}$ variation is determined by the combined effects of the three phenomena.

In the low Reynolds number regime from $Re_c = 1.0 \times 10^4$ to $3.0 \times 10^5$, $C_{L,\max}$ exhibits a weak dependence on $Re_c$, increasing slowly from around 0.8 to 1.0, and the shear layer may reattach on the airfoil surface, forming a separation bubble.[8] The shear layer transition occurs near reattachment, specifically, after reattachment for small $\alpha$ and before for large $\alpha$, as discussed above. The bubble size is prolonged because transition takes place near the reattachment point. The $C_{L,\max}$ is limited by a thin-airfoil stall, i.e., stall type III, where the bubble bursts.[33,40]

The moderate Reynolds number regime covers $Re_c = 3.0 \times 10^5$–$5.0 \times 10^6$. For $\alpha$ near the stall, the shear layer transition occurs between the separation and reattachment points. With increasing $Re_c$, the transition shifts towards the separation point and the separation bubble is shortened. As a result, $C_{L,\max}$ increases rather rapidly, from around 1.0 at $Re_c = 3.0 \times 10^5$–1.6 at $Re_c = 5.0 \times 10^6$. The $C_{L,\max}$ is limited by a leading-edge stall or stall type II, with abrupt flow separation near the leading edge and in general without subsequent reattachment.[33,40]

In the high Reynolds number regime, viz., $Re_c > 5 \times 10^6$, $C_{L,\max}$ displays a weak dependence on $Re_c$ again and is almost a constant of around 1.6. Transition occurs now in the boundary layer prior to separation. An increase in $Re_c$ results in a shift in the boundary layer transition towards the forward stagnation point. $C_{L,\max}$ is less sensitive to $Re_c$ in the absence of a LSB and is limited by a trailing-edge stall, i.e., stall type I.[33,40] The turbulent separation point moves from the trailing to leading edge as $\alpha$ increases.

### C. Flow structure around airfoil

Flow around the airfoil may exhibit different structures with increasing $\alpha$ in each $Re_c$ regime. Eight distinct flow structures have been identified on the suction side of the airfoil, viz.,

A Fully attached laminar boundary layer;
B Partially attached laminar boundary layer which separates near the trailing edge and then rolls up and/or experiences transition further downstream;
C Fully separated laminar shear layer near the leading edge with a subsequent transition downstream but without reattachment;
D Laminar bubble, i.e., laminar flow from separation to reattachment;
E Partially laminar bubble, where laminar separation is followed by turbulent reattachment;
F Fully attached turbulent boundary layer;
G Trailing-edge separated turbulent boundary layer, where flow separation occurs near the trailing edge;
H Fully separated turbulent shear layer where flow separation occurs near the leading edge.

Figure 8 shows schematically these flow structures and the sequence of the flow structures and stall types that occur as $\alpha$ increases in each $Re_c$ regime, that is, A→B→C in the ultra-low $Re_c$ regime, B→D→ E→stall type III→C in the low $Re_c$ regime, E→stall type II→C in the moderate $Re_c$, and F→G →stall type I→H in the high $Re_c$ regime.

These flow structures and their dependence on $Re_c$ and $\alpha$ indicate that shear layer transition, separation and reattachment determine crucially the behaviour of the airfoil wake. In a flow over forward facing steps, Chapman *et al.*[41] concluded that the variable most important to a separated flow is the location of transition relative to reattachment and separation positions. They classified the separated flows into three essentially different types, depending on the relative location of transition: a "pure laminar" type for which transition is downstream of reattachment, a "transitional" type for which transition is between separation and reattachment, and a "turbulent" type for which transition is upstream of separation. Similarly, the occurrence sequence of transition, separation and reattachment determine the flow regimes of the airfoil wake. At very small $\alpha$ and $Re_c$, the laminar boundary layer does not separate from the airfoil, engendering flow structure A, e.g., at $\alpha = 0^\circ$ in Fig. 6. With $\alpha$ and/or $Re_c$ increased, the boundary layer separates before the trailing edge and rolls up behind the trailing edge (e.g., at $\alpha = 2^\circ$ and $5^\circ$ in Fig. 6), that is, flow structure B prevails, causing a linear increase in $C_L$ with a smaller slope (Fig. 4, $Re_c = 5.3 \times 10^3$). When $\alpha$ is large enough, the shear layer separates near the leading edge and rolls up over the surface without reattachment (flow

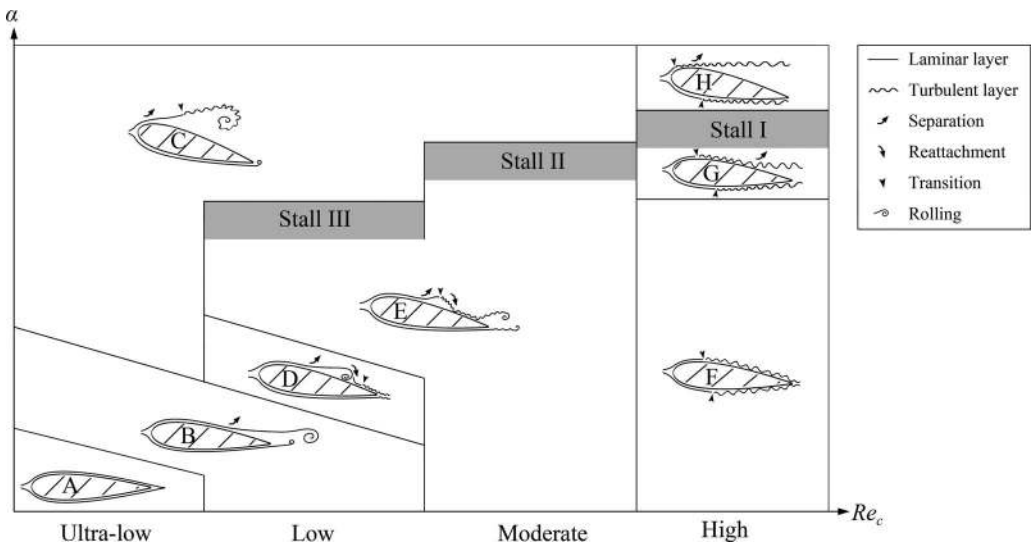


FIG. 8. Schematic of flow structures around airfoil for each $Re_c$ regime.

structure C). This may cause $C_L$ to increase almost linearly or to deteriorate, as illustrated in Fig. 4 for $\alpha > 5^\circ$ in the ultra-low $Re_c$ regime ($Re_c = 5.3 \times 10^3$) and for $\alpha > 10^\circ$ in the low and moderate $Re_c$ regimes ($Re_c = 2.0 \times 10^4$), respectively. Laminar reattachment is possible at small $\alpha$, with transition taking place after reattachment, leading to flow structure D responsible for increasing $dC_L/d\alpha$ from $\alpha = 3^\circ$ to $7^\circ$ at $Re_c = 1.0 \times 10^4$ (Fig. 4). Further increase in $\alpha$ and/or $Re_c$ causes transition before reattachment (Fig. 5(c)) or flow structure E, corresponding to a decreasing $dC_L/d\alpha$. See Fig. 4 for $Re_c = 1.0 \times 10^4$ and $7^\circ < \alpha < 10^\circ$ or $Re_c = 2.0 \times 10^4$ and $\alpha = 3^\circ$–$9^\circ$. If transition occurs before separation, the airfoil is surrounded completely (flow structure F) or partially (flow structure G) by turbulent boundary layer. The latter is associated with the best aerodynamic performance, e.g., achieving the highest $C_{L,\max}$ in the high $Re_c$ regime. A slight increase in $\alpha$, compared with flow structure G, causes turbulent boundary layer separation very near the leading edge or flow structure H.

$Re_c$ plays a crucial role in determining the sequence of shear layer transition, separation, and reattachment. As is well known, given a flow, $Re_c$ is the determining parameter for the transition of the boundary layer. A higher $Re_c$ tends to promote the shear layer transition. For example, the shear layer starts to roll up and transits near the trailing edge at $\alpha = 2^\circ$ for $Re_c = 2.0 \times 10^4$ (Fig. 5(b). On the other hand, the shear layer remains laminar and there is no sign of transition before the trailing edge at the same $\alpha$ for $Re_c = 5.3 \times 10^3$ (Fig. 6). The higher $Re_c$ also promotes flow separation. At $\alpha = 0^\circ$, flow separation occurs on both sides of airfoil at $x^* = 0.9$ for $Re_c = 2.0 \times 10^4$ (Fig. 5(a)) but remains attached for $Re_c = 5.3 \times 10^3$ (Fig. 6). At $\alpha = 2^\circ$, the separation point occurs at $x^* = 0.48$ for $Re_c = 2.0 \times 10^4$ (Fig. 5(b)) but at $x^* = 0.6$ for $Re_c = 5.3 \times 10^3$ (Fig. 6). Similar observations were made both experimentally by Boutilier and Yarusevych[42] and numerically by Kunz and Kroo.[10] As a result of the $Re_c$ effects on separation, transition, and reattachment, the flow structure change at a given pre-stall $\alpha$ follows the sequence of A → B → (D, E) → (F, G) with increasing $Re_c$, as shown in Fig. 8.

## IV. TURBULENT INTENSITY EFFECT

### A. Mean lift, drag, and lift-to-drag ratio

The turbulence level $T_u$ has a significant effect on $C_L$, $C_D$, and $C_L/C_D$ in the ultra-low $Re_c$ regime. Fig. 9 presents the $C_L$, $C_D$, and $C_L/C_D$ variations with $\alpha$ ($\leq 30^\circ$) at $Re_c = 5.3 \times 10^3$. At $T_u = 0.6\%$, $C_L$ increases monotonically with $\alpha$, that is, no separation bubble and hence no stall occurs. At $T_u = 2.6\%$, $C_L$ exceeds that at $T_u = 0.6\%$ over $\alpha = 2^\circ$–$25^\circ$ and shows a rather sharp peak at $\alpha \approx 12^\circ$, suggesting the formation of a separation bubble that bursts at $\alpha \approx 15^\circ$. When stall takes place at $\alpha \approx 12^\circ$, $C_L$ is 38% higher than its counterpart at $T_u = 0.6\%$. The enhancement of $C_L$ as $T_u$ increases is consistent with the results in the literature for the low to moderate $Re_c$

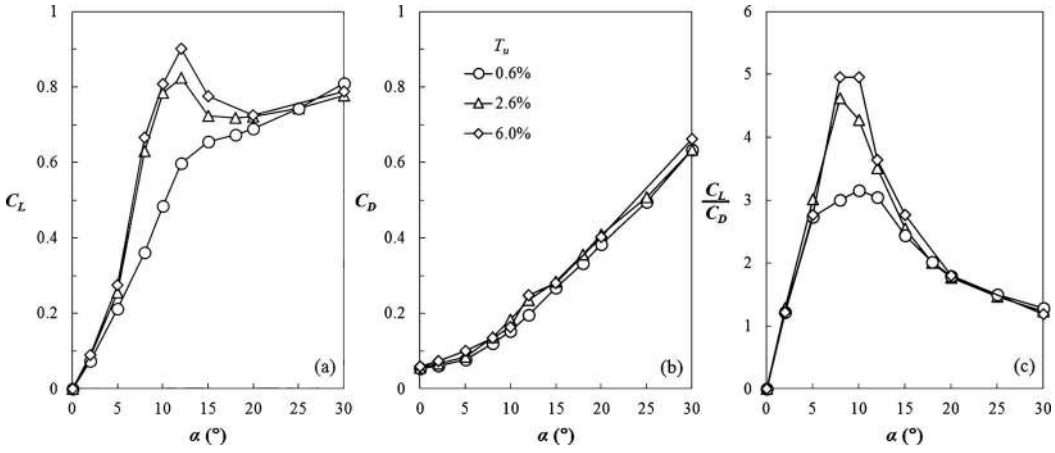


FIG. 9. Dependence on $\alpha$ of $C_L$ (a), $C_D$ (b), and $C_L/C_D$ (c) at different turbulence levels. $Re_c = 5.3 \times 10^3$.

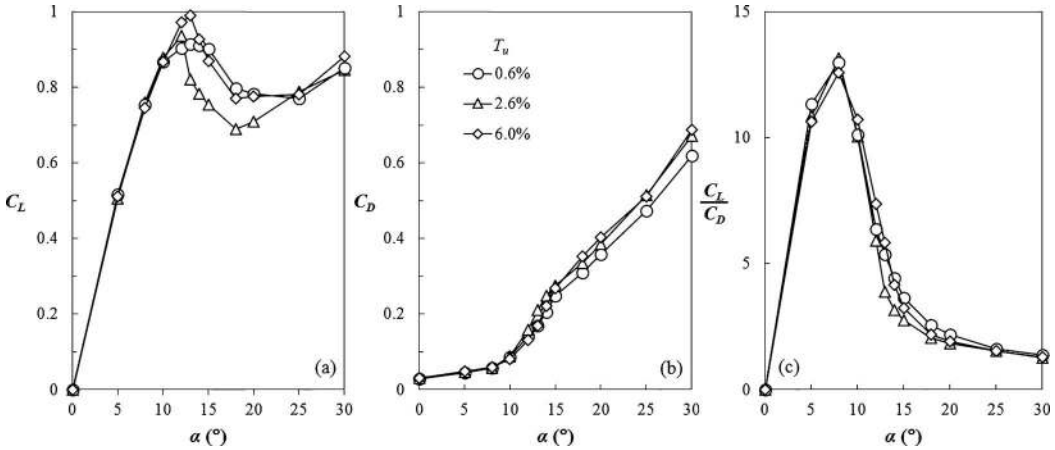


FIG. 10. Dependence of $C_L$ (a), $C_D$ (b), and $C_L/C_D$ (c) on $\alpha$ at different turbulence levels. $Re_c = 2.0 \times 10^4$.

data.[12,43,44] As $T_u$ is further increased to 6.0%, the peak in $C_L$ is more pronounced and 51% higher than that at $T_u = 0.6\%$. The observation suggests that, at least for $Re_c \leq 5.3 \times 10^3$, the stall can occur given adequately high turbulence intensity. It will be shown later that the increased $T_u$ triggers the reattachment of separated flow, thus enhancing $C_L$. The effect of $T_u$ on $C_D$ is less significant. As shown in Fig. 9(b), the measured $C_D$ values of different $T_u$ rise monotonically and almost collapse for $\alpha < 10^\circ$. Note that $C_D$ at $T_u = 6.0\%$ appears increasing more rapidly than at $T_u = 0.6\%$ from $\alpha = 10^\circ$ to $12^\circ$. So does that at $T_u = 2.6\%$. The observation is apparently linked to the occurrence of stall, which is always associated with an increase in drag. The lift-to-drag ratio $C_L/C_D$, proportional to the gliding ratio and climbing ability of the airfoil, is an important parameter to measure the aerodynamic efficiency of airfoil. Fig. 9(c) shows $C_L/C_D$ against $\alpha$ for $Re_c = 5.3 \times 10^3$. Evidently, the increased $T_u$ enlarges the maximum lift-to-drag ratio due to the increased $C_L$, from 3.2 at $\alpha = 10^\circ$ for $T_u = 0.6\%$ to 5.0 at $\alpha = 8^\circ$ for $T_u = 6.0\%$, an increase by 56%.

In the low $Re_c$ regime, the effect of $T_u$ on $C_D$, $C_L$, and $C_L/C_D$ diminishes significantly, as illustrated at $Re_c = 2.0 \times 10^4$ in Fig. 10(a), though qualitatively similar to that in the ultra-low $Re_c$ regime. At $T_u = 0.6\%$, $C_L$ displays a peak, as observed by Alam *et al.*[8] The peak is not sharp, corresponding to the burst of a long separation bubble.[40] The maximum $C_L$ rises by 12% with $T_u$ increasing from 0.6% to 6.0%. This increase is much less than that (51%) at $Re_c = 5.3 \times 10^3$, that is, the influence of $T_u$ is greatly impaired from the ultra-low to the low $Re_c$ regime, consistent with Huang and Lee.[15] At a higher $T_u$, the maximum $C_L$ rises further, though very mildly. However, the peak turns to be sharp, showing a more abrupt drop in $C_L$ at the occurrence of stall. This result suggests a change from the long separation bubble at $Re_c = 5.3 \times 10^3$ to a short one at higher $T_u$ since a sharp fall in $C_L$ corresponds to the leading edge stall characterized by the burst of a short separation bubble.[34,40] With increased $T_u$, $C_D$ varies little from $\alpha = 0^\circ$ to $10^\circ$ (Fig. 10(b)) but displays a discernible increase at $\alpha > 12^\circ$ or after the stall. The observation is linked to the enhanced entrainment of free-stream fluid at higher $T_u$, which may cause a lower pressure in the recirculation region of the wake and give rise to the pressure drag on airfoil. There is little difference in $C_L/C_D$ for different $T_u$ (Fig. 10(c)) due to the cancellation effect of an increase in both $C_L$ and $C_D$.

The above results indicate that the $T_u$ effect on the airfoil wake is more pronounced in the ultra-low $Re_c$ regime because of a difference in the nature of flow separation.

### B. Flow structure

The flow structure captured using qualitative LIF flow visualization and quantitative PIV is presented for $Re_c = 5.3 \times 10^3$ to understand the influence of $T_u$ on the airfoil forces. Fig. 11 compares the flow structure at $T_u = 0.6\%$ and that at $T_u = 6.0\%$. The laminar boundary layer remains completely attached to the airfoil at $\alpha = 0^\circ$ (Figs. 11(a) and 11(i)) but appears separated

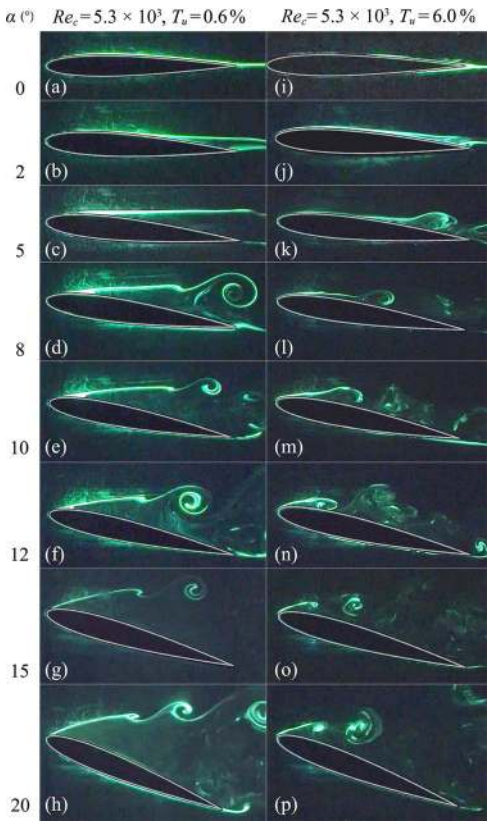


FIG. 11. Typical photographs captured in LIF flow visualization for various $\alpha$.

near the trailing edge at $\alpha = 2^\circ$ (Figs. 11(b) and 11(j)) for both $T_u$ levels. The observation suggests that the laminar boundary layer cannot withstand even a slight adverse pressure gradient that is present at $\alpha < 2^\circ$ in the ultra-low $Re_c$ regime. The separation point occurs at $0.60c$ and $0.63c$ from the leading edge for $T_u = 0.6\%$ and 6.0%, respectively, that is, the increased $T_u$ acts to postpone flow separation, albeit slightly. The postponed separation is more evident at $\alpha = 5^\circ$, where flow separation takes place at $0.23c$ from the leading edge at $T_u = 0.6\%$ (Fig. 11(c)) but at $0.45c$ at $T_u = 6.0\%$ (Fig. 11(k)).

The separated shear layer develops more difference downstream. At $\alpha = 2^\circ$, the upper shear layer is laminar for $T_u = 0.6\%$ (Fig. 11(b)) without reattachment or mixing with the lower shear layer, at least within the extent of the image. But this layer appears mixed with the lower shear layer at the trailing edge for $T_u = 6.0\%$ (Fig. 11(j)). This mixing suggests an enhanced entrainment ability of the wake due to the increased $T_u$. At $\alpha = 5^\circ$, the upper shear layer at $T_u = 0.6\%$ remains laminar for a long distance without reattachment (Fig. 11(c)). But at $T_u = 6.0\%$ (Fig. 11(k)), the shear layer appears rolling up and experiencing transition shortly after separation and reattaches the airfoil surface at $0.8c$ from the leading edge. Obviously, the transition to turbulence has been advanced as a result of the increased $T_u$. The fact that the increased $T_u$ acts to promote the shear layer transition is more evident at larger $\alpha$. For example, at $\alpha = 15^\circ$, the transition occurs at around $0.5c$ from the leading edge for $T_u = 0.6\%$ (Fig. 11(g)) but at $0.2c$ for $T_u = 6.0\%$ (Fig. 11(o)). The advanced transition enhances greatly the entrainment and broadens the shear layer, resulting in reattachment. For both levels of $T_u$, the transition approaches gradually the separation point with $\alpha$ increased further, as reported.[42,45]

Note that, at $T_u = 0.6\%$, the separated shear layer does not reattach the airfoil surface for any $\alpha$ presently examined (Figs. 11(d)–11(h)), in agreement with Sunada *et al.*[46] observation from flow visualization over $\alpha = 6^\circ$–$16^\circ$ at $Re_c = 4 \times 10^3$ for the same airfoil. At $T_u = 6.0\%$, in contrast, the separated shear layer reattaches at $\alpha \geq 5^\circ$, producing a separation bubble. From $\alpha = 5^\circ$ to $12^\circ$,

the reattachment point moves gradually towards the leading edge and the separation bubble appears shrinking in size (Figs. 11(k)–11(n)). However, the upper shear layer fails to reattach the airfoil surface at $\alpha \geq 15^\circ$ (Figs. 11(o) and 11(p)). As a result, the separation bubble disappears or bursts, forming a large recirculation zone.

The physical picture now emerges, which depends on the $T_u$ level. For the ultra-low $Re_c$ and low $T_u$, the separation point of the upper boundary layer moves from the trailing edge to the leading edge with increasing $\alpha$; the separated shear layer remains laminar for a relatively long distance. As shown in Fig. 8, the flow structure change follows the pattern of A → B → C in the ultra-low $Re_c$ regime. However, for the high $T_u$ level, the upper separation point shifts towards the leading edge less rapidly, and the shear layer becomes turbulent shortly after separation. As such, the flow structure change follows the pattern of A → B → D → E → C, which is almost the same as in the low $Re_c$ regime. The observation suggests some similarity in flow changes when increasing $T_u$ and $Re_c$, respectively, which will be discussed along with disparity in Sec. V.

## V. DISCUSSION

### A. Similarity between the $Re_c$ and $T_u$ effects

As noted earlier, the effect of increasing $T_u$ shows similarity to that of increasing $Re_c$. They both alter the $C_L$ dependence on $\alpha$, resulting in larger slope and $C_{L,\max}$ and hence a higher lift-to-drag ratio. Take the $C_L$–$\alpha$ relationship at $Re_c = 5.3 \times 10^3$ and $T_u = 0.6\%$ (Fig. 12) as a reference, which is almost linear up to $\alpha = 12^\circ$. The $C_L$–$\alpha$ relationship at $T_u = 2.6\%$ appears quite similar to that at $Re_c = 1.0 \times 10^4$ for pre-stall $\alpha$, with increasing and decreasing $dC_L/d\alpha$ from $\alpha = 3^\circ$ to $7^\circ$ and $7^\circ$ to $12^\circ$, respectively, which are connected to laminar and partially-laminar bubbles. In both cases, an earlier transition occurs in shear layer, causing flow reattachment and forming a separation bubble. The formation of the bubble has a positive effect on the aerodynamic performance of airfoil, increasing the maximum lift. When $Re_c$ was further increased, the inflection point where $dC_L/d\alpha$ changes from increasing to decreasing is shifted, from $\alpha = 7^\circ$ at $Re_c = 1.0 \times 10^4$ to $\alpha = 3^\circ$ at $Re_c = 2.0 \times 10^4$. A similar observation is made, with the inflection point shifted to $5^\circ$, when $T_u$ is increased to 6.0%. In spite of a difference in pre-stalled $C_L$ between $Re_c = 2.0 \times 10^4$ ($T_u = 0.6\%$) and $T_u = 6.0\%$

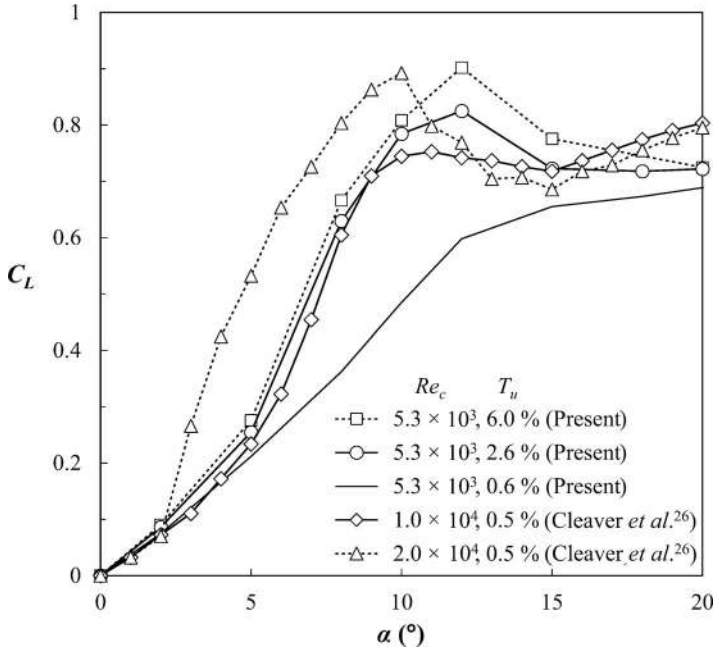


FIG. 12. Comparison between the $Re_c$ and $T_u$ effects on $C_L$.

($Re_c = 5.3 \times 10^3$), $C_{L,\max}$ is enlarged to the same degree. It may be concluded that the effect of increasing $Re_c$ bears close similarity to that increasing $T_u$.

### B. Scaling parameter of the maximum lift

Quantitative equivalent relationship between $T_u$ and $Re_c$ could be established at least to some extent since increasing $T_u$ produces almost the same effect as increasing $Re_c$, e.g., forming a separation bubble, enhancing transition in the shear layer, shifting the inflection point to lower $\alpha$ and enlarging $C_{L,\max}$. As far as $C_{L,\max}$ is concerned, the effect of a larger $T_u$ can be treated as an addition of $Re_c$, that is, $C_{L,\max}$ at a lower $Re_c$ and a non-zero $T_u$ is equivalent to that at a higher $Re_c$ and zero $T_u$.

This similarity was recognized in the moderate and high $Re_c$ regimes as early as 1930s. Dryden and Kuethe[47] found that increasing $T_u$ caused a decrease in the critical Reynolds number, $Re_{d,\mathrm{cr}}$ based on diameter $d$, of the sphere wake, at which the transition occurred in the boundary layer and drag coefficient dropped greatly, that is, increasing $T_u$ hastened the transition in the boundary layer. They concluded that the flow about the sphere at a low Reynolds number in a wind tunnel was like that at a high Reynolds number in a non-turbulent stream. They conducted a similar test on streamlined airship models and predicted that the same concept could be applied to airfoil models. Inspired by this, Jacobs and Clay[48] referred to the low Reynolds number in a turbulent stream as the test Reynolds number $Re$ ($Re_d$ for the sphere and $Re_c$ for the airfoil) and called the corresponding high Reynolds number, at which the similar flow state could occur in a non-turbulent stream, as the effective Reynolds number $Re_{\mathrm{eff}}$ ($Re_{d,\mathrm{eff}}$ for the sphere and $Re_{c,\mathrm{eff}}$ for the airfoil). He defined a turbulence factor $TF$, viz.,

$$TF = \mathrm{Re}_{\mathrm{eff}}/\mathrm{Re} \tag{3}$$

and assumed it to be dependent only on $T_u$. $TF$ serves to connect $Re_c$ and $Re_{c,\mathrm{eff}}$ and removes the $T_u$ effect. Once the $TF$-$T_u$ correlation is established, the corresponding $Re_{\mathrm{eff}}$ could be determined from Eq. (3) for a given $Re$ and $T_u$. Obviously, given $T_u = 0$, $TF$ equals 1, resulting in $Re_{\mathrm{eff}} = Re$; $TF$ grows with increasing $T_u$. Jacobs suggested two ways to determine $TF$, that is, comparing either the dependence of $C_D$ on $Re_d$ of the sphere wake or the dependence of $C_{L,\max}$ on $Re_c$ of the airfoil wake obtained in a wind tunnel ($T_u \neq 0$) with that in flight tests conducted in free air ($T_u = 0$). The $TF$ values determined from the two methods agreed with each other for the flight $Re$ range, i.e., $Re > 1.0 \times 10^5$,[32,47] though a possible difference may exist for $Re < 1.0 \times 10^5$.[48] The agreement lies in the fact that a higher $T_u$ may incur the transition in the boundary layer, thus postponing flow separation, and this flow physics may affect equally the $C_D$-$Re_d$ and $C_{L,\max}$-$Re_c$ correlations. The sphere cylinder wake data are often used because the $T_u$ effect may be easily quantified in terms of a change in $Re_{d,\mathrm{cr}}$, at which $C_D$ drops abruptly. In contrast, there have been few attempts to use the airfoil wake data. First, a Reynolds number has yet to be identified, which is representative, unique, and sensitive to the $T_u$ effect in the moderate to high $Re_c$ regimes. Second, the $C_{L,\max}$ data base of various $T_u$ is inadequate for the determination of $TF$. Based on Dryden and Kuethe's empirical correlation between $Re_{d,\mathrm{cr}}$ and $T_u$ in the sphere wake,[47] and the assumption that the effect of turbulence on the boundary layer transition is approximately the same for spheres and airfoils, Platt[49] applied $TF = 3.85 \times 10^5/Re_{d,\mathrm{cr}}$, where $3.85 \times 10^5$ is the $Re_{d,\mathrm{cr}}$ in free air, for the airfoil wake at flight $Re_c$. Thus obtained correlations between $C_{L,\max}$ and $Re_{c,\mathrm{eff}}$ collapsed into a single curve,[32,48,49] albeit from a number of different wind tunnels with various $T_u$.

It would be interesting to know whether the data of $C_{L,\max}$ vs. $Re_{c,\mathrm{eff}}$ could collapse into one curve in the ultra-low and low $Re_c$ regimes. We failed to see this collapse when $Re_{c,\mathrm{eff}}$ was calculated from $TF = 3.85 \times 10^5/Re_{d,\mathrm{cr}}$. For example, at $Re_c = 2.0 \times 10^4$ and $T_u = 0.6\%$, reattachment occurs on the upper surface (Sec. IV). $Re_{d,\mathrm{cr}}$ would be $2.6 \times 10^5$ at $T_u = 0.6\%$ based on data from Dryden and Kuethe,[47] and $TF = 3.85 \times 10^5/Re_{d,\mathrm{cr}} = 3.85 \times 10^5/2.6 \times 10^5 = 1.5$. Then, the corresponding $Re_{c,\mathrm{eff}}$ should be $Re_c TF = 2.0 \times 10^4 \times 1.5 = 3.0 \times 10^4$, that is, a similar reattached flow should occur in a non-turbulent stream at an effective Reynolds number of $3.0 \times 10^4$. This is contradictory to the suggestion from Carmichael[50] that the minimum Reynolds number for the occurrence of reattachment is $5.0 \times 10^4$ in a non-turbulent stream for most common airfoils. A

similar contradiction is found at $Re_c = 5.3 \times 10^3$. The $T_u$ effect on the airfoil wake is grossly underestimated in the ultra-low and low $Re_c$ regimes if the classical $TF$ ($=3.85 \times 10^5/Re_{d,\mathrm{cr}}$) is simply applied. It may be concluded that the classical $TF$-$T_u$ correlation, based on the sphere wake data, cannot be extended to the low and ultra-low $Re_c$ regimes. Physically, $Re_{d,\mathrm{cr}}$ occurs only at the moderate to high $Re_c$ and cannot be connected to the $T_u$ effect at very low $Re_c$. This verifies the assertion from Jacobs and Sherman[32] that the classical $TF$ was suitable only over the flight range of the Reynolds number. They did not examine the range of Reynolds Number below the usual flight range, though recognizing its fundamental importance, due to a lack of practical applications at that time, along with the poor measurement accuracy in low Reynolds number airfoil experiments.

One may naturally beg the question how to determine $TF$ in the ultra-low and low $Re_c$ regimes. To this end, we propose to compare $Re_{c,\mathrm{cr}}$, identified from the dependence of $C_{L,\max}$ on $Re_c$, obtained in a wind tunnel ($T_u \neq 0$) with its counterpart in free air ($T_u = 0$). The choice of $Re_{c,\mathrm{cr}}$ is due to a number of considerations. First, unlike $Re_{d,\mathrm{cr}}$, $Re_{c,\mathrm{cr}}$ lies in the $Re_c$ range of concern. Second, $Re_{c,\mathrm{cr}}$ is the critical Reynolds number between the ultra-low and low $Re_c$ regimes and is easy to identify. As shown in the dependence of $C_{L,\max}$ on $Re_c$ (Fig. 7), there is an abrupt increase in $C_{L,\max}$ at $Re_{c,\mathrm{cr}}$ with rising $Re_c$. Also, there is one pronounced peak (stall) for $Re_c > Re_{c,\mathrm{cr}}$ but none for $Re_c < Re_{c,\mathrm{cr}}$ in the $C_L$ dependence on $\alpha$ (Fig. 4). Third, $Re_{c,\mathrm{cr}}$ in free air ($T_u = 0$) could be estimated from previously reported data, which is crucial to determine quantitatively the relationship of $TF = TF(Re_{c,\mathrm{cr}})$. Based on his comprehensive survey of test data from different laboratories, Carmichael[50] stated that, for most common airfoils, under natural laminar separation conditions, the distance from separation to reattachment could be expressed as $Re_\mathrm{R}$ - $Re_\mathrm{S} = 5.0 \times 10^4$, where $Re_\mathrm{R}$ and $Re_\mathrm{S}$ were chord Reynolds numbers based on distances from the leading edge to the separation and reattachment points, respectively. We may then infer $Re_{c,\mathrm{cr}} = 5.0 \times 10^4$ in free air in view of the definition of $Re_{c,\mathrm{cr}}$. Finally, a number of $Re_{c,\mathrm{cr}}$ is available for various $T_u$ from present measurements and previous reports, allowing the variation in $Re_{c,\mathrm{cr}}$ to be correlated with $T_u$. Huang and Lin[51] classified the characteristic flow modes of NACA 0012 for $Re_c = 3.0 \times 10^3$–$1.2 \times 10^5$ in a wind tunnel with $T_u = 0.2\%$, suggesting a $Re_{c,\mathrm{cr}}$ between $2.0 \times 10^4$ and $4.0 \times 10^4$. The present LIF and PIV data clearly indicates the formation of a LSB for $Re_c = 2.0 \times 10^4$ and the absence of the bubble for $Re_c = 5.3 \times 10^3$ at $T_u = 0.6\%$, suggesting a $Re_{c,\mathrm{cr}}$ between $2.0 \times 10^4$ and $5.3 \times 10^3$. Similarly, the $Re_{c,\mathrm{cr}}$ is estimated to be less than $5.3 \times 10^3$ at $T_u = 2.6\%$ and 6.0% based on the observed formation of LSBs.

Fig. 13 presents the correlation between $Re_{c,\mathrm{cr}}$ and $T_u$, where the upper and lower bars indicate the range of uncertainty. Evidently, $Re_{c,\mathrm{cr}}$ drops rapidly as $T_u$ increases from 0% to 0.6% and then

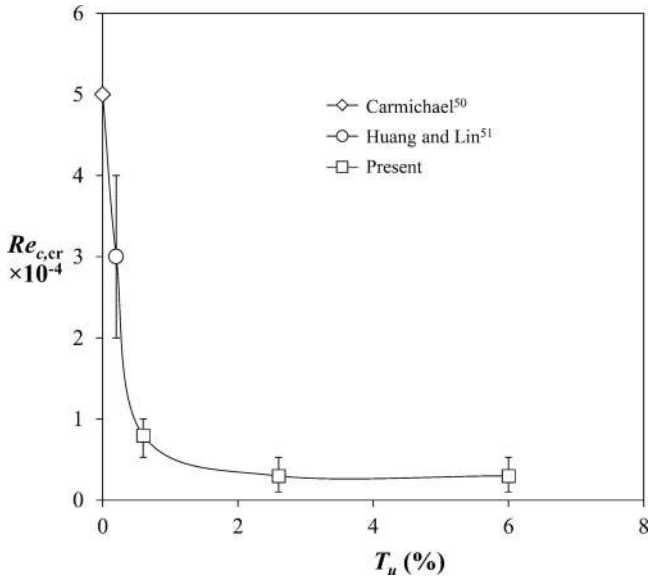


FIG. 13. Dependence on $T_u$ of the critical Reynolds number $Re_{c,\mathrm{cr}}$, which divides the ultra-low and low $Re_c$ regimes.

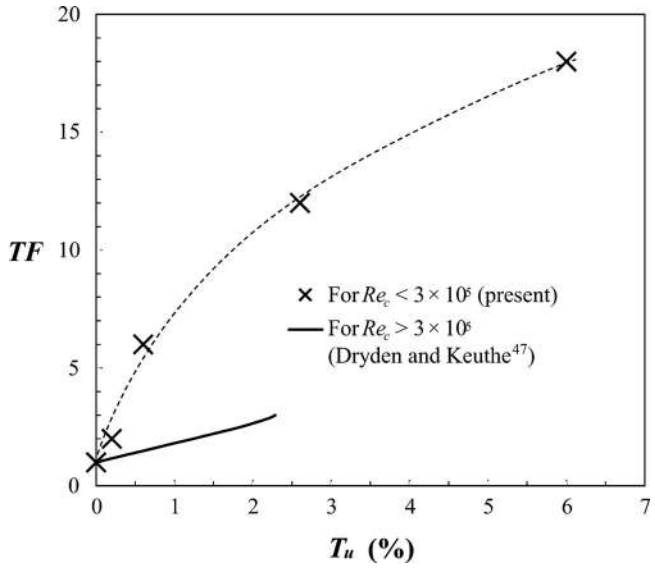


FIG. 14. Dependence of turbulence factor $TF$ on $T_u$ for NACA 0012 in the ultra-low and low $Re_c$ regimes.

slowly for higher $T_u$. This is because at a higher $T_u$ a smaller $Re_c$ is required to promote the transition in the shear layer. Noting that $TF \equiv Re_{c,\text{eff}}/Re_c$ and $Re_{c,\text{eff}} = Re_c = 5.0 \times 10^4$ at $T_u = 0$ based on Fig. 13, we may find

$$TF = 5.0 \times 10^4 / Re_{c,\text{cr}}. \tag{4}$$

In arriving at Eq. (4), we have invoked the assumption that $TF$ is dependent only on $T_u$. In view of the relation between $Re_{c,\text{cr}}$ and $T_u$ (Fig. 13), we may correlate $TF$ and $T_u$ from Eq. (4), as shown in Fig. 14. This relation is good for the ultra-low to low $Re_c$ regimes of the airfoil wake. The classical data of $TF$, obtained from the sphere wake, is also given in the figure, which is valid only for the moderate to high $Re_c$ regimes.[48] Despite of different methods involved in determining $TF$, their physical implication should be the same for the two $TF$ curves. The $TF$ is significantly larger in the ultra-low to low $Re_c$ regimes than in the moderate to high $Re_c$ regimes, highlighting the enhanced $T_u$ effect in the former regimes. From Eq. (3), we then have

$$Re_{c,\text{eff}} = Re_c \times (3.85 \times 10^5 / Re_{d,\text{cr}}), \quad Re_c > 3.0 \times 10^5, \tag{5a}$$

$$Re_{c,\text{eff}} = Re_c \times (5.0 \times 10^4 / Re_{c,\text{cr}}), \quad Re_c < 3.0 \times 10^5. \tag{5b}$$

Figure 15(a) presents the variation in $C_{L,\max}$ with $Re_{c,\text{eff}}$, collected from the literature as well as ours. The data from Jacobs and Sherman[32] cover the moderate and high $Re_c$ regimes. Most of the data collapse essentially into a single curve, in distinct contrast to the considerable scattering in the $C_{L,\max}$-$Re_c$ relation (Fig. 15(b)). A certain degree of departure is expected; after all, the data were measured in different facilities using different techniques. The observation demonstrates unequivocally that $C_{L,\max}$ is scaled with $Re_{c,\text{eff}}$. Note that the $C_{L,\max}$-$Re_{c,\text{eff}}$ relationship agrees qualitatively with that between $C_{L,\max}$ and $Re_c$ (Fig. 7), thus providing a validation for the presently estimated $TF$, which is crucial for establishing the equivalence between $Re_c$ and $T_u$ in the airfoil wake of the ultra-low to low $Re_c$ regimes. The critical $Re_{c,\text{eff}}$ that divides the ultra-low and low $Re_c$ regimes in the ideal non-turbulent free-stream ($T_u = 0$) is $5.0 \times 10^4$, which is 5 times $Re_{c,\text{cr}}$ (Fig. 7) obtained from actual experimental conditions ($0 < T_u \leq 1\%$). Similarly, the other two critical Reynolds numbers that separate the low, moderate, and high Reynolds number regimes are also shifted to larger values in the ideal non-turbulent free-stream: from $3 \times 10^5$ and $5 \times 10^6$ to $8 \times 10^5$ and $6 \times 10^6$, respectively. In view of the physical meaning of $Re_{c,\text{eff}}$, Fig. 15 presents the dependence of $C_{L,\max}$ on the Reynolds number in the ideal non-turbulent free-stream.

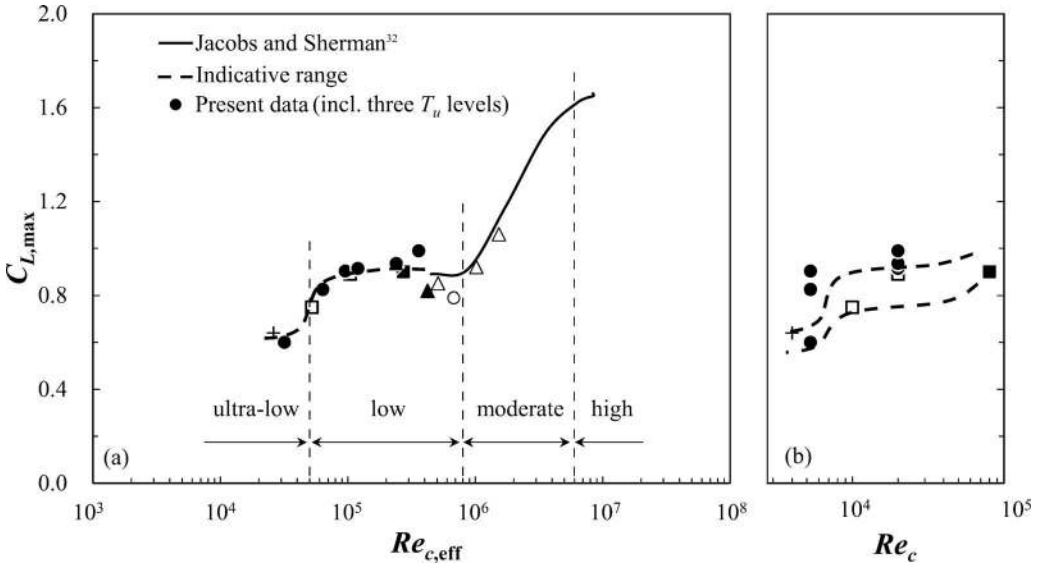


FIG. 15. Dependence of the maximum lift coefficient $C_{L,\max}$ on (a) effective Reynolds number $Re_{c,\text{eff}}$, (b) test Reynolds number $Re_c$: + Sunada *et al.*[25]; ■ Chen and Choa[35]; □ Cleaver *et al.*[26]; ◯ Grager *et al.*[36]; ♦ Lee and Gerontakos[37]; ▲ Wong and Kontis[38]; △ Sant and Ayuso.[39]

### C. Difference between the $Re_c$ and $T_u$ effects

The influences of $T_u$ and $Re_c$ on flow separation are opposite to each other. An increase in $T_u$ postpones flow separation; yet an increase in $Re_c$ promotes early separation, followed by reattachment. To our best knowledge, this has not been reported previously. Fig. 16 presents instantaneous snapshots of the flow structure captured from LIF flow visualization and the iso-contours of PIV-measured $\overline{U}^*$, where the effect of increasing $Re_c$ on the separation point is compared with that of increasing $T_u$ ($\alpha = 5^\circ$). As indicated in the snapshots, the separation point is postponed from $0.23c$, from the leading edge, at $T_u = 0.6\%$ (Fig. 16(c)) to $0.45c$ at $T_u = 6.0\%$ (Fig. 16(a)). On the other hand, given $T_u = 0.6\%$, this point moves from $0.23c$ at $Re_c = 5.3 \times 10^3$ to $0.18c$ at $Re_c = 2.0 \times 10^4$ (Fig. 16(e)). The $\overline{U}^*$-contours re-confirm this observation. Note that, for given $Re_c$ and $T_u$ (e.g., Figs. 16(a) and 16(b)), the separation points identified from the instantaneous PIV images and the $\overline{U}^*$-contours may not occur at exactly the same position because of the unsteady nature of the separation point.

The normalized separation point position $x^*_{\text{sep}}$ from the leading edge, extracted from the time-averaged PIV data, depends on $\alpha$, as summarized in Fig. 17. The separation point moves to the leading edge with increasing $\alpha$, irrespective of the combination of $T_u$ and $Re_c$. The separation point at $Re_c = 5.3 \times 10^3$ moves closer to the leading edge from $T_u = 0.6\%$ to 6.0%. However, given $T_u = 0.6\%$, this point moves in the opposite direction from $Re_c = 5.3 \times 10^3$ to $2.0 \times 10^4$, indicating the opposite effect of increasing $T_u$ and increasing $Re_c$ on the separation point at $\alpha = 5^\circ$–$20^\circ$.

This opposite effect was also observed on a SD7003 airfoil in low $Re_c$ range ($Re_c = 2.1 \times 10^4$–$4.6 \times 10^4$) by Olson *et al.*,[52] though without any explanation. Aubertine[53] investigated the effect of Reynolds number on the adverse pressure gradient boundary layer developed along a 4° ramp and noted an increasing adverse pressure gradient with increasing Reynolds number. This may provide a clue on the present observation, that is, increased $Re_c$ may incur an increase in the adverse pressure gradient and hence early separation. On the other hand, as $T_u$ grows from 0.6% (Fig. 16(d)) to 6.0% (Fig. 16(b)), the occurrence of $\overline{U}^*_{\max}$, though changing little in magnitude, is shifted appreciably downstream. So is the separation position. The increased $T_u$ can enhance the mixing of the boundary layer with high momentum free-stream fluid, resulting in the postponed flow separation.

Both flow structure and stall depend not only on $Re_c$ and $T_u$ but also on the airfoil shape including thickness, camber, etc. The shape effect on the flow structure can be different for different

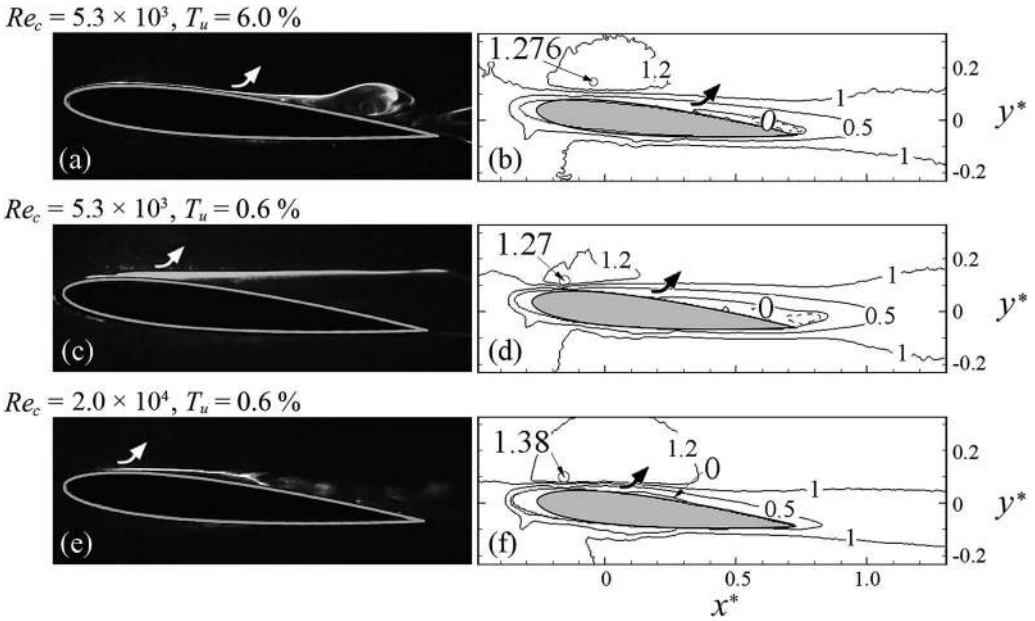


FIG. 16. Effect of $Re_c$ or $T_u$ on the flow separation point at $\alpha = 5^\circ$. Left column: photographs of instantaneous flow structure captured from LIF flow visualization; right column: iso-contours of PIV-measured time-averaged streamwise velocity $\overline{U}^*$. Symbol ↗ indicates the occurrence of flow separation.

$Re_c$ regimes. The shape effect can be significant, influencing the transition, separation, reattachment, etc., in the moderate and high $Re_c$ regimes where the boundary layer is attached/reattached over a longer length of the airfoil at relatively large $\alpha$ than in the other two regimes (Fig. 8). In the other two $Re_c$ regimes, in particular at ultra-low $Re_c$, the boundary layer separates at smaller $\alpha$, with transition occurring late in the free shear layer (Fig. 8). Once the boundary layer is separated, the afterbody shape has little influence on flow. The deterioration of the aerodynamic performance in the ultra-low $Re_c$ regime is primarily due to the absence of the separation bubble. A simple change

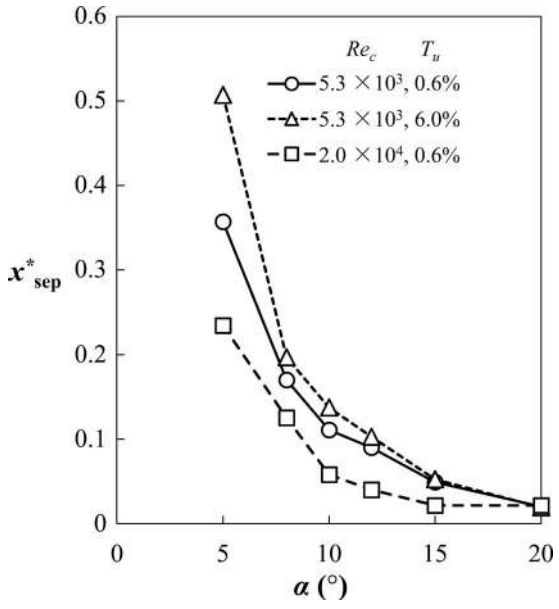


FIG. 17. Dependence of the flow separation point $x^*_{sep}$ on $\alpha$.

in the airfoil geometry, such as increasing camber or moving the position of the maximum camber backwards, may not effectively promote the transition or formation of bubble, and therefore may not affect significantly the airfoil performance.

### D. Criteria for bursting of the separation bubble

Gaster developed a general criteria in 1967 for predicting conditions that lead to a burst of short separation bubble.[54] He studied a laminar separation bubble on flat plate and proposed a criterion to predict when the short bubble will burst into long bubble. The method is based on two parameters, the momentum-thickness Reynolds number ($Re_{\theta,\mathrm{sep}}$) and a dimensionless velocity gradient (sometimes called a dimensionless pressure gradient and hence denoted by $\Delta P_{\mathrm{avg}}$),

$$\Delta P_{\mathrm{avg}} = \frac{\theta_{\mathrm{sep}}^2}{\nu}\frac{\Delta U}{\Delta x}. \tag{6}$$

The velocity gradient can be obtained from an inviscid flow analysis without separation. Gaster obtained this gradient by measuring the pressure distribution when the separation has been inhibited by tripping the boundary layer, which is an approximation to the inviscid pressure distribution if the boundary layer thickness is negligible.

As the present investigation involves the onset and burst of the laminar separation bubble, it is of interest to examine whether the general separation criteria still hold in the ultra-low to low Reynolds number regimes. The momentum thickness of the boundary layer at separation and the length of the separation bubble can be estimated from PIV-measured time-averaged velocity. Following discussion is made first on the characteristics of the time-averaged LSB and then on the correlation criteria.

Fig. 18 shows typical PIV-measured time-averaged velocity vectors and the $\bar{U}$-contours of the separation bubble at $\alpha = 5^\circ$ ($Re_c = 2.0 \times 10^4$), which clearly outline the shape of LSB. The scale in the $y$ direction is enlarged to improve the visibility of the bubble. As discussed earlier, the boundary layer changes from laminar to turbulent between the separation and reattachment points. The normalized velocity ($U^*_{\mathrm{e}}$) at the outer edge of the boundary layer, minimum streamwise velocity ($U^*_{\mathrm{min}}$, associated with reversed flow) and momentum thickness ($\theta$) on the suction side of the airfoil were estimated and plotted against $x/c$ in Fig. 19. Inviscid velocity distribution is included in Fig. 19 for the purpose of comparison, obtained using Xfoil, a commonly used and well validated code in airfoil analysis by Drela.[55] The major characteristics of LSB can be easily extracted as follows. The maximum $U^*_{\mathrm{e}}$ near the leading edge represents the suction peak. Flow passing beyond the suction peak encounters an adverse pressure gradient, but remains attached until the separation point. $U^*_{\mathrm{e}}$

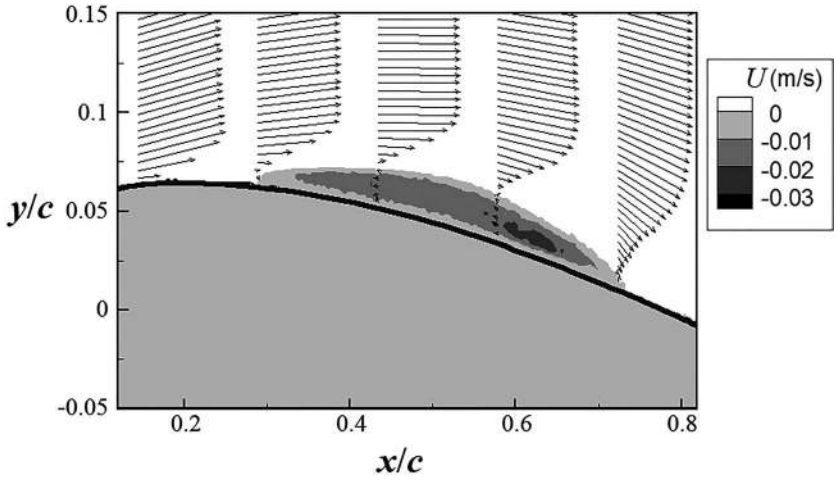


FIG. 18. Velocity vectors and the $\bar{U}$-contours of the separation bubble at $\alpha = 5^\circ$. $Re_c = 2.0 \times 10^4$. The scales of $x$ and $y$ are different.

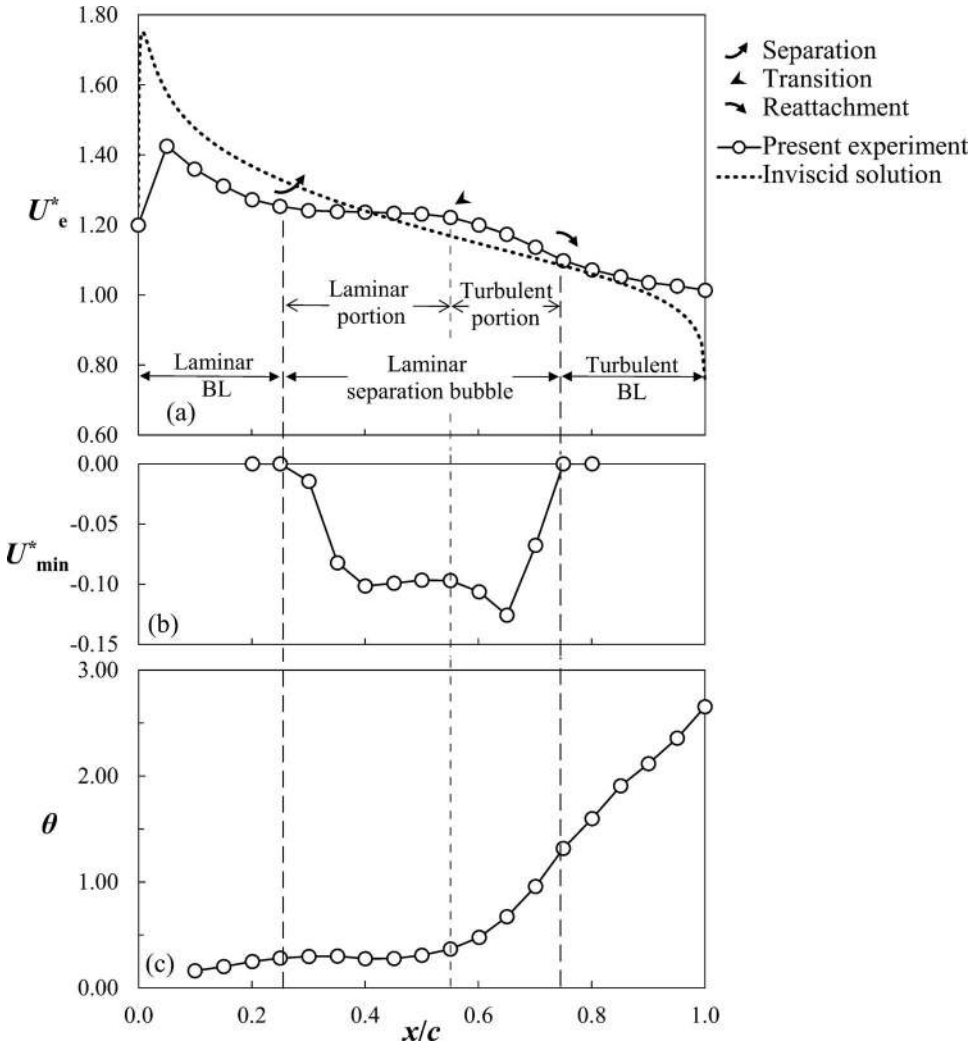


FIG. 19. (a) Normalized boundary layer edge velocity $U^*_e$, (b) normalized minimum velocity $U^*_{min}$, and (c) momentum thickness $\theta$ of the boundary layer at $\alpha = 5^\circ$. $Re_c = 2.0 \times 10^4$.

decreases and $\theta$ increases gradually along $x/c$ in this area. Starting from the separation point, $U^*_e$ and $\theta$ maintain constant up to the transition point. $U^*_{min}$ drops from zero to a negative value at first, and then tends to be constant in this $x/c$ range. After the transition occurs in the separated boundary layer, turbulent mixing reduces $U^*_e$, resulting in reattachment. In the turbulent region, $\theta$ grows rapidly, while $U^*_{min}$ first drops to a minimum value and then recovers to zero, which is in agreement with Gaster's measurements.[54] After reattachment, the turbulent boundary layer forms, with mildly decreasing $U^*_e$, increasing $\theta$ and zero $U^*_{min}$.

The normalized length of LSB ($L^*_{LSB}$) and momentum thickness at separation ($\theta_{sep}$) are plotted against $\alpha$ for cases where LSB was visible, as shown in Fig. 20. As $\alpha$ climbs, $L^*_{LSB}$ retreats to a minimum value before the bubble bursts for both flow conditions, i.e., $Re_c = 5.3 \times 10^3$ at $T_u = 6.0\%$ and $Re_c = 2.0 \times 10^4$ at $T_u = 0.6\%$. Following Gaster's definition,[54] we refer to the condition at which $L^*_{LSB}$ reaches the minimum as the critical point for the LSB bursting. Under both flow conditions, $\theta_{sep}$ drops with increasing $\alpha$, resulting from the forward-shifted separation point.

Figure 21 compares the presently obtained $\Delta P_{avg}$ with the criterion curve proposed by Gaster. As shown by the solid line, his criterion curve does not include data for $Re_{\theta,sep} < 130$. A simple extrapolation of this curve to lower $Re_{\theta,sep}$, marked by the dashed curve, results in considerably lower $\Delta P_{avg}$ than the present result, denoted by the dotted line. This indicates a failure to apply Gaster's

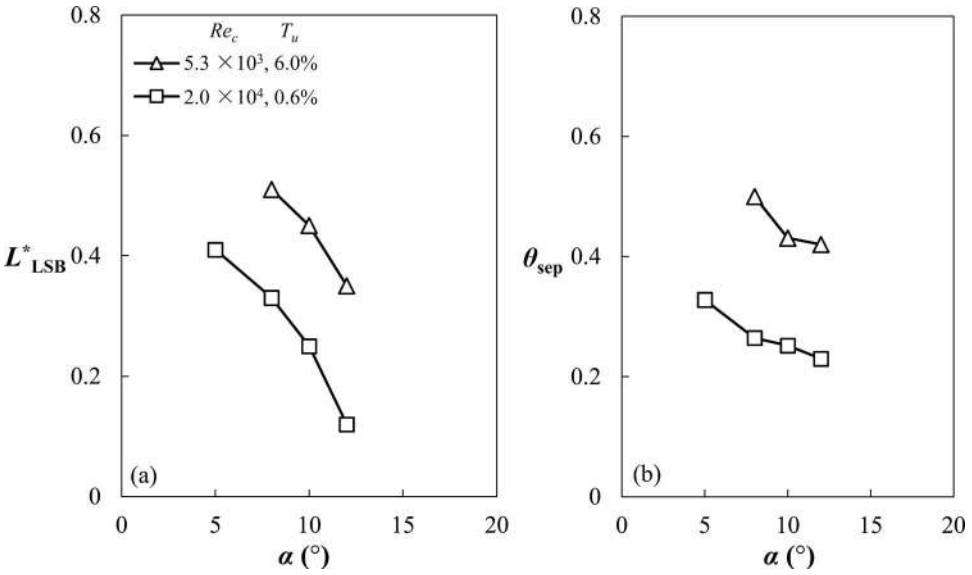


FIG. 20. Dependence of the laminar separation bubble (LSB) on $\alpha$: (a) normalized bubble length $L^*_{\mathrm{LSB}}$ and (b) momentum thickness $\theta_{\mathrm{sep}}$ of the boundary layer at separation.

bursting criterion to the low and ultra-low $Re_c$ regimes. One possible reason for the large discrepancy may come from the estimate of $\Delta P_{\mathrm{avg}}$. Gaster obtained this value by tripping the laminar boundary layer to a turbulent one, which remained attached, rather than by the direct inviscid analysis of the pressure distribution. The inviscid analysis is based on the ideal airfoil section and dismisses the displacement effect of the actual boundary layer, but the experimental tripped-boundary-layer method is affected by the thickness of actual boundary layer. Though the deviation produced by the two methods is negligible for the moderate to high $Re_c$ regimes due to a thin boundary layer, it is not so for the ultra-low to low $Re_c$ regimes, because the displacement effect of the boundary layer cannot be neglected, where the boundary layer thickness is rather thick.

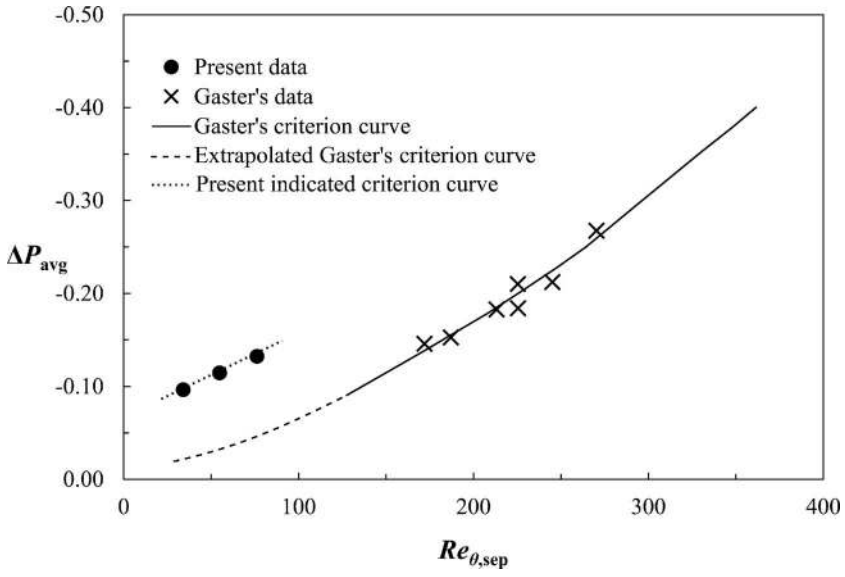


FIG. 21. Relation between $Re_{\theta,\mathrm{sep}}$ and $\Delta P_{\mathrm{avg}}$ at bursting.

## VI. CONCLUSIONS

Investigation has been experimentally carried out on the aerodynamics in the wake of an NACA 0012 airfoil for $Re_c = 5.3 \times 10^3$ and $2.0 \times 10^4$. Following conclusions can be drawn:

(1) Four $Re_c$ regimes have been proposed for the first time, i.e., the ultra-low ($<1.0 \times 10^4$), low ($1.0 \times 10^4$–$3.0 \times 10^5$), moderate ($3.0 \times 10^5$–$5.0 \times 10^6$), and high ($>5.0 \times 10^6$) regimes, each exhibiting distinct characteristics in terms of its $C_{L,\max}$-$Re_c$ relationship and flow structure dependence on $\alpha$. The separated laminar shear layer does not reattach in the ultra-low $Re_c$ regime but does, forming a separation bubble, in the low $Re_c$ regime. The transition to turbulence occurs after reattachment at small $\alpha$ and before reattachment at large $\alpha$. The moderate $Re_c$ regime is also associated with a separation bubble, though the transition takes place before reattachment, closer to the separation point. On the other hand, the transition occurs in the boundary layer, prior to flow separation, in the high $Re_c$ regime.

(2) In the four $Re_c$ regimes, eight distinct flow structures are observed on the suction side of the airfoil, namely, flow structures A (fully attached laminar boundary layer), B (partially attached laminar boundary layer), C (fully separated laminar shear layer), D (laminar bubble), E (partially laminar bubble), F (fully attached turbulent boundary layer), G (trailing-edge-separated turbulent boundary layer), and H (fully separated turbulent shear layer). With increasing $\alpha$, the flow structure changes and the sequence is A→B→C in the ultra-low $Re_c$ regime, B→D →E→stall type I→C in the low $Re_c$ regime, E→stall type II→C in the moderate $Re_c$, and F→G →stall type III→H in the high $Re_c$ regime.

(3) All the $C_L$ data collapses for $\alpha < 2^\circ$–$5^\circ$, with the exact $\alpha$ range depending on $Re_c$ and increases for a smaller $Re_c$, in the ultra-low and low $Re_c$ regimes. The corresponding slope $dC_L/d\alpha$ is 0.038, different from the well-known slope of 0.11 for an airfoil at small $\alpha$ in the high $Re_c$ regime. The laminar and turbulent boundary layers attaching on most of the airfoil lead to the former and latter slopes, respectively. For $\alpha > 2^\circ$–$5^\circ$, $C_L$ increases almost linearly to $C_{L,\max}$ in the ultra-low $Re_c$ regime and nonlinearly in the low $Re_c$ regime where $dC_L/d\alpha$ may increase and decrease. While the linear variation is associated with the rollup of laminar shear layer over the airfoil surface without reattachment, the increasing and decreasing $dC_L/d\alpha$ are connected to reattaching shear layer with transition after and before reattachment, respectively.

(4) In the ultra-low $Re_c$ regime, the influence of $T_u$ is significant. Stall does not occur at $T_u = 0.6\%$ but does at $T_u = 2.6\%$ and 6.0%. With increased $T_u$, flow separation is postponed and the transition occurs in the separated shear layer, which may induce flow reattachment and improve significantly the aerodynamic performance of airfoil. For example, at $Re_c = 5.3 \times 10^3$, the maximum $C_L$ and $C_L/C_D$ can be increased by 52% and 45%, respectively, from $T_u = 0.6\%$ to 6.0%. This increase is comparable with that due to increasing $Re_c$ in the ultra-low $Re_c$ regime. In the low $Re_c$ regime, the $T_u$ effect wanes. For example, stall occurs at $Re_c = 2.0 \times 10^4$, regardless of the level of $T_u$. The maximum $C_L$ is increased by only 10% and the maximum $C_L/C_D$ does not even change from $T_u = 0.6\%$ to 6.0%.

(5) The influence of $T_u$ on the airfoil wake exhibits similarity to that of $Re_c$. Given a higher value, both $T_u$ and $Re_c$ may increase $C_{L,\max}$ or maximum $C_L/C_D$ and may cause early transition in the shear layer and hence reattachment, forming a separation bubble. As such, the concept of the effective Reynolds number, which treats $T_u$ as additional $Re_c$ in the moderate and high $Re_c$ regimes, is extended and validated in the low and ultra-low $Re_c$ regimes. Nevertheless, there is a difference between the two effects. The increased $T_u$ postpones flow separation due to enhanced mixing; but the increased $Re_c$ causes a more pronounced adverse pressure gradient, which changes little with $T_u$, in the boundary layer and thus promotes flow separation.

(6) It has been found that $C_{L,\max}$ at different $T_u$ displays considerable scattering if plotted against $Re_c$ but collapses into one single curve if $Re_c$ is replaced by $Re_{c,\text{eff}}$, that is, $C_{L,\max}$ is scaled with $Re_{c,\text{eff}}$ ($=TF\,Re_c$). While $Re_{c,\text{eff}}$ was estimated based on the critical Reynolds number, at which the transition occurs in the boundary layer of the sphere wake, for the moderate and high $Re_c$ regimes, it is presently determined based on the critical Reynolds number $Re_{c,\text{cr}}$ that divides the ultra-low and low $Re_c$ regimes and is given by $Re_{c,\text{eff}} = 5.0 \times 10^4/Re_{c,\text{cr}}$. The

$Re_{c,\mathrm{cr}}$ depends strongly on $T_u$, decreasing rapidly from $5.0 \times 10^4$ at $T_u = 0$ to $7.8 \times 10^3$ at $T_u = 0.6\%$ and then displays a slow drop to $5.3 \times 10^3$ at $T_u = 6.0\%$.

(7) A simple extrapolation of the classical two-parameter bursting criterion for short laminar separation bubble does not apply to present cases in ultra-low and low $Re_c$ regimes. A new criterion line is suggested to be validated for $Re_{\theta,\mathrm{sep}}$ less than 100, where $Re_{\theta,\mathrm{sep}}$ is the momentum thickness based Reynolds number at the separation of boundary layer.

## ACKNOWLEDGMENTS

Y.Z. wishes to acknowledge support given to him by Research Grants Council of HKSAR through Grant No. PolyU 5329/11E and by National Science Foundation of China through Grant No. 50930007. M.M.A. acknowledges support given to him by Shenzhen Research Grant No. (JCYJ20130402100505796).

[1] M. Brendel and T. J. Mueller, "Boundary-layer measurements on an airfoil at a low Reynolds-number in an oscillating freestream," AIAA J. **26**(3), 257–263 (1988).
[2] F.-B. Hsiao, C.-F. Liu, and Z. Tang, "Aerodynamic performance and flow structure studies of a low Reynolds number airfoil," AIAA J. **27**(2), 129–137 (1989).
[3] J. C. M. Lin and L. L. Pauley, "Low-Reynolds-number separation on an airfoil," AIAA J. **34**(8), 1570–1577 (1996).
[4] T. J. Mueller, "Aerodynamic measurements at low Reynolds numbers for fixed wing micro-air vehicles," DTIC No. ADP010760, 1999.
[5] D. Pines, "Nano air vehicle (nav) program," in *Proposer Information Pamphlet for Defense Advanced Research Projects Agency*, edited by D. A. R. P. Agency (BAA, 2005).
[6] Z. J. Wang, "Dissecting insect flight," Annu. Rev. Fluid. Mech. **37**(1), 183–210 (2005).
[7] T. J. Mueller and J. D. DeLaurier, "Aerodynamics of small vehicles," Annu. Rev. Fluid. Mech. **35**(1), 89–111 (2003).
[8] M. M. Alam, Y. Zhou, H. X. Yang, H. Guo, and J. Mi, "The ultra-low Reynolds number airfoil wake," Exp. Fluids **48**(1), 81–103 (2010).
[9] Y. Zhou, M. M. Alam, H. X. Yang, H. Guo, and D. H. Wood, "Fluid forces on a very low Reynolds number airfoil and their prediction," Int. J. Heat Fluid Fl. **32**(1), 329–339 (2011).
[10] P. Kunz and I. Kroo, "Analysis, design, and testing of airfoils for use at ultra-low Reynolds numbers," in *Fixed, Flapping and Rotary Wing Vehicles at Very Low Reynolds Numbers*, edited by T. J. Mueller (AIAA, Reston, VA, 2001).
[11] P. J. Mckeough and J. M. R. Graham, "Effect of mean loading on the fluctuating loads induced on aerofoils by a turbulent stream," Aeronaut. Quart. **31**, 56–69 (1980).
[12] J. A. Hoffmann, "Effects of freestream turbulence on the performance characteristics of an airfoil," AIAA J. **29**(9), 1353–1354 (1991).
[13] P. F. Mish and W. J. Devenpor, "Mean loading effects on the surface pressure fluctuations on an airfoil in turbulence," AIAA Paper No. 2001-2211, 2001.
[14] L. Gilling, N. S. rensen, and L. Davidson, "Detached eddy simulations of an airfoil in turbulent inflow," AIAA Paper No. 2009-270, 2009.
[15] R. F. Huang and H. W. Lee, "Effects of freestream turbulence on wing-surface flow and aerodynamic performance," J. Aircraft **36**(6), 965–972 (1999).
[16] P. Devinant, T. Laverne, and J. Hureau, "Experimental study of wind-turbine airfoil aerodynamics in high turbulence," J. Wind Eng. Ind. Aerod. **90**(6), 689–707 (2002).
[17] J. Colman, J. M. Di Leo, J. S. Delnero, M. Martinez, U. Boldes, and F. Bacchi, "Lift and drag coefficients behaviour at low Reynolds number in an airfoil with gurney flap submitted to a turbulent flow. Part 1," Lat. Am. Appl. Res. **38**(3), 195–200 (2008).
[18] H. F. Wang, Y. Zhou, C. K. Chan, and K. S. Lam, "Effect of initial conditions on interaction between a boundary layer and a wall-mounted finite-length-cylinder wake," Phys. Fluids **18**(6), 065106 (2006).
[19] J. Hoffmann, "Effects of onset free-stream turbulence on the performance characteristics of an airfoil," AIAA Paper No. 90-3025, 1990.
[20] C. Sicot, S. Aubrun, S. Loyer, and P. Devinant, "Unsteady characteristics of the static stall of an airfoil subjected to freestream turbulence level up to 16%," Exp. Fluids **41**(4), 641–648 (2006).
[21] E. C. Maskell, "A theory of the blockage effects on bluff bodies and stalled wings in a closed wind tunnel," Aeronautical Research Council Reports and Memoranda No. 3400, 1963.
[22] J. B. Barlow, W. H. Rae, and A. Pope, *Low-Speed Wind Tunnel Testing*, 3rd ed. (Wiley, 1999).
[23] W. J. McCroskey, "A critical assessment of wind tunnel results for the NACA 0012 airfoil," NASA TM No. 100019, 1987.
[24] A. Host-Madsen and D. McCluskey, "On the accuracy and reliability of piv measurements," DTIC Report No. ADA285647, 26.4.1–26.4.11, 1994.
[25] S. Sunada, K. Kawachi, K. Yasuda, and T. Yasuda, "Comparison of wing characteristics at an ultralow Reynolds number," J. Aircraft **39**(2), 331–338 (2002).
[26] D. J. Cleaver, Z. Wang, I. Gursul, and M. R. Visbal, "Lift enhancement by means of small-amplitude airfoil oscillations at low Reynolds numbers," AIAA J. **49**(9), 2018–2033 (2011).
[27] C. C. Critzos, H. H. Heyson, and J. Boswinkle, W. Robert, "Aerodynamic characteristics of NACA 0012 airfoil section at angles of attack from 0 to 180 degrees," NACA TN No. 3361, 1955.

[28] M. M. Munk, "Elements of the wing section theory and of the wing theory," NACA Report No. 191, 1924.
[29] J. Panda, and K. B. M. Q. Zaman, "Experimental investigation of the flow field of an oscillating airfoil and estimation of lift from wake surveys," J. Fluid. Mech. **265**, 65–95 (1994).
[30] E. V. Laitone, "Wind tunnel tests of wings at Reynolds numbers below 70 000," Exp. Fluids **23**(5), 405–409 (1997).
[31] T. Lutz, W. Würz, and S. Wagner, "Numerical optimization and wind-tunnel testing of low Reynolds number airfoils," in *Fixed, Flapping and Rotary Wing Vehicles at Very Low Reynolds Numbers*, edited by T. J. Mueller (AIAA, Reston, VA, 2001).
[32] E. N. Jacobs and A. Sherman, "Airfoil section characteristics as affected by variations of the Reynolds number," NACA Report No. 586, 1937.
[33] D. E. Gault, "A correlation of low-speed, airfoil-section stalling characteristics with Reynolds number and airfoil geometry," NACA TN No. 3963, 1957.
[34] E. C. Polhamus, "A survey of Reynolds number and wing geometry effects on lift characteristics in the low speed stall region," NASA CR No. 4745, 1996.
[35] J. M. Chen and C.-C. Choa, "Freestream disturbance effects on an airfoil pitching at constant rate," J. Aircraft **36**(3), 507–514 (1999).
[36] T. Grager, A. Rothmayer, and H. Hu, "Stall suppression of a low-Reynolds-number airfoil with a dynamic burst control plate," AIAA Paper No. 2011-1180, 2011.
[37] T. Lee and P. Gerontakos, "Investigation of flow over an oscillating airfoil," J. Fluid Mech. **512**, 313–341 (2004).
[38] C. Wong and K. Kontis, "Flow control by spanwise blowing on a NACA 0012," J. Aircraft **44**(1), 338–341 (2007).
[39] R. Sant, L. Ayuso, and J. Meseguer, "Aerodynamic study of airfoils geometric imperfections at low Reynolds number," AIAA Paper No. 2011–1256 (2011).
[40] G. B. McCullough and D. E. Gault, "Examples of three representative types of airfoil section stall at low speeds," NACA TN No. 2502 (1951).
[41] D. R. Chapman, D. M. Kuehn, and H. K. Larson, "Preliminary report on a study of separated flows in supersonic and subsonic streams," NACA RM No. A55L 14, 1956.
[42] M. S. H. Boutilier and S. Yarusevych, "Parametric study of separation and transition characteristics over an airfoil at low Reynolds numbers," Exp. Fluids **52**(6), 1491–1506 (2012).
[43] P. F. Mish and W. J. Devenport, "An experimental investigation of unsteady surface pressure on an airfoil in turbulence—Part 1: Effects of mean loading," J. Sound Vib. **296**(3), 417–446 (2006).
[44] P. F. Mish and W. J. Devenport, "An experimental investigation of unsteady surface pressure on an airfoil in turbulence—Part 2: Sources and prediction of mean loading effects," J. Sound Vib. **296**(3), 447–460 (2006).
[45] S. Yarusevych, J. G. Kawall, and P. E. Sullivan, "Separated-shear-layer development on an airfoil at low Reynolds numbers," AIAA J. **46**(12), 3060–3069 (2008).
[46] S. Sunada, A. Sakaguchi, and K. Kawachi, "Airfoil section characteristics at a low Reynolds number," J. Fluids Eng. **119**(1), 129–135 (1997).
[47] H. L. Dryden and A. M. Kuethe, "Effect of turbulence in wind tunnel measurements," NACA Report No. 342, 1931.
[48] E. N. Jacobs and W. C. Clay, "Characteristics of the NACA 23012 airfoil from tests in the full-scale and variable-density tunnels," NACA Report No. 530, 1936.
[49] R. C. Platt, "Turbulence factors of NACA wind tunnels as determined by sphere tests," NACA Report No. 558, 1936.
[50] B. H. Carmichael, "Low Reynolds number airfoil survey, volume 1," NASA CR No. 165803, 1981.
[51] R. F. Huang and C. L. Lin, "Vortex shedding and shear-layer instability of wing at low-Reynolds numbers," AIAA J. **33**(8), 1398–1403 (1995).
[52] D. Olson, A. Katz, A. Naguib, M. Koochesfahani, D. Rizzetta, and M. Visbal, "On the challenges in experimental characterization of flow separation over airfoils at low Reynolds number," Exp. Fluids **54**(2), 1470 (2013).
[53] C. D. Aubertine, Ph.D. thesis, Stanford University, 2005.
[54] M. Gaster, "The structure and behaviour of laminar separation bubbles," A.R.C. R.&M. No. 5395, 1967.
[55] M. Drela and M. B. Giles, "Viscous-inviscid analysis of transonic and low Reynolds number airfoils," AIAA J. **25**(10), 1347–1355 (1987).